Cytoplasmic mRNA decay represses RNA polymerase II transcription during early apoptosis

Christopher Duncan-Lewis[1], Ella Hartenian[1], and Britt A. Glaunsinger*[1,2,3]

GRAPHICAL ABSTRACT

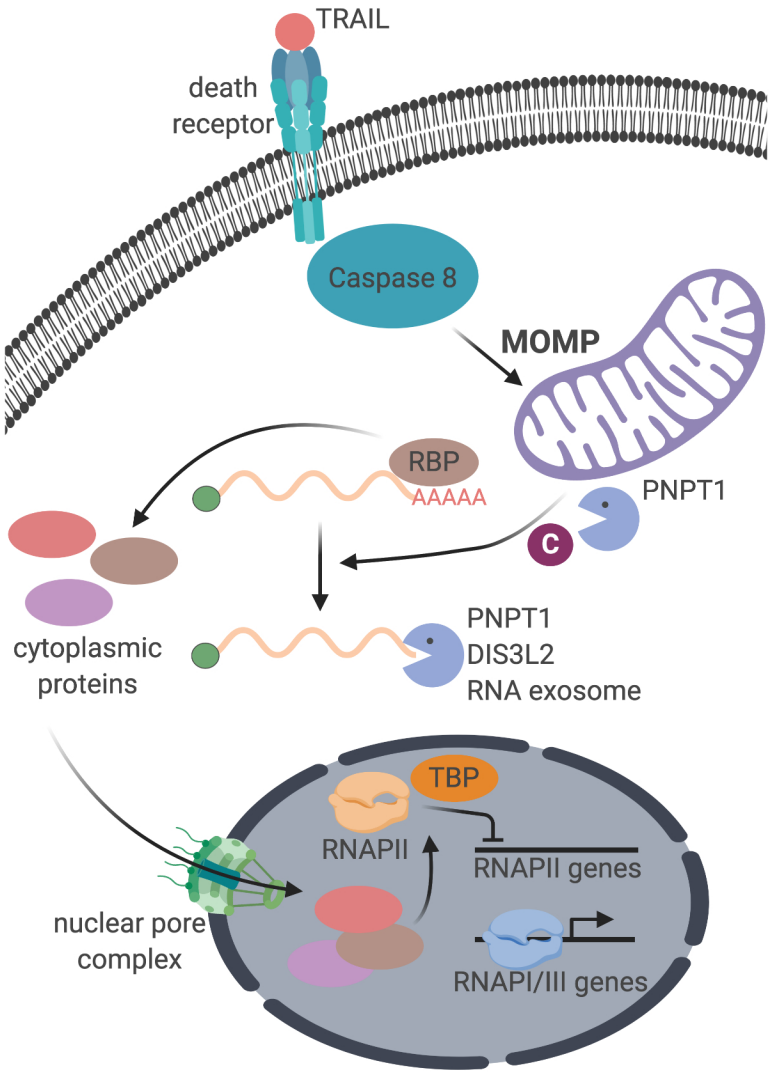

[1] Department of Molecular and Cell Biology; University of California, Berkeley; Berkeley, CA 94720, USA
[2]Department of Plant and Microbial Biology; University of California, Berkeley; Berkeley, CA 94720, USA
[3]Howard Hughes Medical Institute, Berkeley, CA 94720, USA
*Correspondence: glaunsinger@berkeley.edu

SUMMARY

RNA abundance is generally sensitive to perturbations in decay and synthesis rates, but crosstalk between RNA polymerase II transcription and cytoplasmic mRNA degradation often leads to compensatory changes in gene expression. Here, we reveal that widespread mRNA decay during early apoptosis represses RNAPII transcription, indicative of positive (rather than compensatory) feedback. This repression requires active degradation of cytoplasmic mRNA, which leads to impaired recruitment of components of the transcription preinitiation complex to promoter DNA. Importin α/β-mediated nuclear import is critical for this feedback signaling, suggesting that proteins translocating between the cytoplasm and nucleus connect mRNA decay to transcription. We also show that an analogous pathway activated by viral nucleases similarly depends on nuclear protein import. Collectively, these data demonstrate that accelerated mRNA decay leads to the repression of mRNA transcription, thereby amplifying the shutdown of gene expression. This highlights a conserved gene regulatory mechanism by which cells respond to threats.

KEYWORDS

mRNA decay, transcription, apoptosis, nuclear transport

INTRODUCTION

The central dogma of molecular biology depicts gene expression as a unidirectional flow of discrete stages: DNA is first transcribed by RNA polymerase II (RNAPII) into messenger RNA (mRNA), which is processed and exported to the cytoplasm where it is translated and then degraded. However, there is a growing body of work that reveals complex cross talk between the seemingly distal steps of

29 transcription and decay. For example, the yeast Ccr4-Not deadenylase complex, which
30 instigates basal mRNA decay by removing the poly(A) tails of mRNAs (Tucker et al.,
31 2001), was originally characterized as a transcriptional regulator (Collart and Stmhp,
32 1994; Denis, 1984). Other components of transcription such as RNAPII subunits and
33 gene promoter elements have been linked to cytoplasmic mRNA decay (Bregman et al.,
34 2011; Lotan et al., 2007, 2005), while the activity of cytoplasmic mRNA degradation
35 machinery such as the cytoplasmic 5'-3' RNA exonuclease Xrn1 can influence the
36 transcriptional response (Haimovich et al., 2013; Sun et al., 2012).

37 The above findings collectively support a model in which cells engage a buffering
38 response to reduce transcription when mRNA decay is slowed, or reduce mRNA decay
39 when transcription is slowed to preserve the steady state mRNA pool (Haimovich et al.,
40 2013; Hartenian and Glaunsinger, 2019). While much of this research has been
41 performed in yeast, the buffering model is also supported by studies in mouse and
42 human cells (Helenius et al., 2011; Singh et al., 2019). In addition to bulk changes to the
43 mRNA pool, compensatory responses can also occur at the individual gene level to
44 buffer against aberrant transcript degradation. Termed "nonsense-induced transcription
45 compensation" (NITC; Wilkinson, 2019), this occurs when nonsense-mediated mRNA
46 decay leads to transcriptional upregulation of genes with some sequence homology to
47 the aberrant transcript (El-Brolosy et al., 2019; Ma et al., 2019).

48 A theme that unites much of the research linking mRNA decay to transcription is
49 homeostasis; perturbations in mRNA stability are met with an opposite transcriptional
50 response in order to maintain stable mRNA transcript levels. However, there are cellular
51 contexts in which homeostasis is not beneficial, for example during viral infection. Many

52 viruses induce widespread host mRNA decay (Narayanan and Makino, 2013) and co-
53 opt the host transcriptional machinery (Harwig et al., 2017) in order to express viral
54 genes. Indeed, infection with mRNA decay-inducing herpesviruses or expression of
55 broad-acting viral ribonucleases in mammalian cells causes RNAPII transcriptional
56 repression in a manner linked to accelerated mRNA decay (Abernathy et al., 2015;
57 Hartenian et al., 2020). It is possible that this type of positive feedback represents a
58 protective cellular shutdown response, perhaps akin to the translational shutdown
59 mechanisms that occur upon pathogen sensing (Walsh et al., 2013). A central question,
60 however, is whether transcriptional inhibition upon mRNA decay is restricted to infection
61 contexts, or whether it is also engaged upon other types of stimuli.
62 The best-defined stimulus known to broadly accelerate cytoplasmic mRNA
63 decay outside of viral infection is induction of apoptosis. Overall levels of poly(A) RNA
64 are reduced rapidly after the induction of extrinsic apoptosis via accelerated degradation
65 from the 3' ends of transcripts (Thomas et al., 2015). The onset of accelerated mRNA
66 decay occurs coincidentally with mitochondrial outer membrane depolarization (MOMP),
67 and requires release of the mitochondrial exonuclease polyribonucleotide
68 nucleotidyltransferase 1 (PNPT1) into the cytoplasm. PNPT1 then coordinates with
69 other 3' end decay machinery such as DIS3L2 and terminal uridylyltransferases
70 (TUTases; Liu et al., 2018; Thomas et al., 2015). Notably, mRNA decay occurs before
71 other hallmarks of apoptosis including phosphatidylserine (PS) externalization and DNA
72 fragmentation, but likely potentiates apoptosis by reducing the expression of unstable
73 anti-apoptotic proteins such as MCL1 (Thomas et al., 2015).

74 Here, we used early apoptosis as a model to study the impact of accelerated
75 cytoplasmic mRNA decay on transcription. We reveal that under conditions of increased
76 mRNA decay, there is a coincident decrease in RNAPII transcription, indicative of
77 positive feedback between mRNA synthesis and degradation. Using decay factor
78 depletion experiments, we demonstrate that mRNA decay is required for the
79 transcriptional decrease and further show that transcriptional repression is associated
80 with reduced RNAPII polymerase occupancy on promoters. This phenotype requires
81 ongoing nuclear-cytoplasmic protein transport, suggesting that protein trafficking may
82 provide the signal linking cytoplasmic decay to transcription. Collectively, our findings
83 elucidate a distinct gene regulatory mechanism by which cells sense and respond to
84 threats.

85 **RESULTS**

86 ***mRNA decay during early apoptosis is accompanied by reduced synthesis of***
87 ***RNAPII transcripts***

88 To induce widespread cytoplasmic mRNA decay, we initiated rapid extrinsic
89 apoptosis in HCT116 colon carcinoma cells by treating them with TNF-related apoptosis
90 inducing ligand (TRAIL). TRAIL treatment causes a well-characterized progression of
91 apoptotic events including caspase cleavage and mitochondrial outer membrane
92 permeabilization or “MOMP” (Albeck et al., 2008; Thomas et al., 2015). It is caspase 8
93 (CASP8)-induced MOMP that stimulates mRNA decay in response to an apoptosis-
94 inducing ligand (Figure 1A), partly by releasing the mitochondrial 3’-5’ RNA exonuclease
95 PNPT1 into the cytoplasm (Liu et al., 2018; Thomas et al., 2015). A time course
96 experiment in which cells were treated with 100 ng/mL TRAIL for increasing 30 min

97 increments showed activation of CASP8 and caspase 3 (CASP3) by 1.5 hr, as
98 measured by disappearance of the full-length zymogen upon cleavage (Figure 1B). In
99 agreement with Liu et al. (2018), RT-qPCR performed on total RNA revealed a
100 coincident decrease in the mRNA levels of several housekeeping genes (*ACTB*,
101 *GAPDH*, *EEF1A*, *PPIA, CHMP2A, DDX6, RPB2, and RPLP0*) beginning 1.5 hr after
102 TRAIL was applied (Figures 1C, S1A). As expected, this decrease was specific to
103 RNAPII transcripts, as the RNA polymerase III (RNAPIII)-transcribed ncRNAs *U6*, *7SK,*
104 *7SL, and 5S* did not show a similarly progressive decrease. The *U6* transcript was
105 instead upregulated, possibly suggesting post-transcriptional regulation of *U6* as alluded
106 to in a previous study (Noonberg et al., 1996). These data confirm that mRNA depletion
107 occurs by 1.5-2 hr during TRAIL-induced apoptosis.
108 To monitor whether apoptosis also influenced transcription, we pulse labeled the
109 cells with 4-thiouridine (4sU) for 20 min at the end of each TRAIL treatment. 4sU is
110 incorporated into actively transcribing RNA and can be subsequently coupled to HPDP-
111 biotin and purified over streptavidin beads, then quantified by RT-qPCR to measure
112 nascent transcript levels (Dölken, 2013). This revealed that in addition to a reduction in
113 steady state mRNA abundance, TRAIL treatment caused a decrease in RNAPII-driven
114 mRNA production, while RNAPIII transcription was either unaffected or enhanced
115 (Figures 1D, S1B). Thus, early apoptosis triggers mRNA decay and decreases nascent
116 mRNA production but does not negatively impact RNAPIII transcript abundance or
117 production.
118 ***Transcriptional repression during early apoptosis requires MOMP but is not***
119 ***directly dependent on caspase activity***

120 We next sought to determine whether any hallmark features of apoptosis
121 underlay the observed transcriptional repression. These include limited proteolysis by
122 the “initiator” CASP8, mass proteolysis by the “executioner” CASP3, and the
123 endonucleolytic cleavage of the genome by caspase-activated DNase (CAD), which
124 translocates into the nucleus during late stages of apoptosis (Enari et al.,1998).
125 To evaluate the contribution of caspases to this phenotype, HCT116 cells were
126 pre-treated with 40 μM z-VAD-fmk (zVAD, a pan-caspase inhibitor) for 1 hr prior to
127 TRAIL treatment. The effectiveness of zVAD treatment was confirmed by showing it
128 blocked the CASP8-mediated cleavage of BID as well as the degradation of the CASP3
129 substrate PARP1 (Figure S2A). The decreases in mRNA levels upon TRAIL treatment
130 were rescued in the presence of zVAD (Figure 2A), confirming a role for one or more
131 caspases in activating mRNA decay during TRAIL-induced apoptosis. Nascent mRNA
132 production was also rescued upon zVAD treatment, as measured by 4sU pulse labeling
133 during the last 20 min of treatment (Figure 2B).
134 Small interfering RNA (siRNA) knock downs of CASP8 and CASP3 (Figure 2C)
135 were then performed to determine if the rescue of mRNA production caused by zVAD
136 was due specifically to the inhibition of the initiator CASP8 or the executioner CASP3.
137 Both accelerated mRNA decay (Figure S2B) and RNAPII transcriptional repression
138 (Figure 2D) required CASP8 but not CASP3, suggesting that mass proteolysis by
139 CASP3 does not significantly contribute to either phenotype. Knock down of CAD did
140 not affect the reduction in 4sU incorporation observed during early apoptosis (Figure
141 2D), and DNA fragmentation (as measured by TUNEL assay) was not detected in
142 TRAIL-treated HCT116 cells until 4-8 hr post-treatment (Figure S2C). These findings

143 are in agreement with the prior study showing that MOMP-induced mRNA decay occurs
144 before DNA fragmentation begins during extrinsic apoptosis (Thomas et al., 2015).
145 Although CASP3 is dispensable for apoptotic transcriptional repression, a
146 previous report suggests that CASP8 may cleave RPB1, the largest subunit of RNAPII
147 (Lu et al., 2002). We therefore measured the protein expression of RPB1 and the 3 next
148 largest RNAPII subunits (RBP2-4) during early apoptosis to determine if degradation of
149 these subunits might explain the observed TRAIL-induced reduction in RNAPII
150 transcription. Western blots probing for RPB1 showed no significant decrease in protein
151 levels upon TRAIL treatment between 1 and 3 hr (Figure S2D). Furthermore, levels of
152 RPB1-4 were relatively unaffected by 2 hr TRAIL treatment in the presence or absence
153 of zVAD, with the exception of a small decrease in the amount of RPB2 that was
154 rescued upon zVAD treatment (Figure S2E).
155 Finally, to determine if the activity of any caspase was at all required for apoptotic
156 mRNA decay and ensuing transcriptional repression, we used a small molecule,
157 raptinal, that bypasses CASP8 to intrinsically stimulate MOMP (Palchaudhuri et al.,
158 2015). HeLa cells treated with 10 μM raptinal for 4 hr underwent MOMP, as measured
159 by cytochrome c release into the cytoplasm, in the presence or absence of zVAD
160 (Figure S2E). Steady state levels and transcription of the *ACTB* and *GAPDH* mRNAs
161 were reduced upon raptinal treatment, and this reduction in mRNA abundance and
162 synthesis was maintained upon caspase inhibition by zVAD treatment (Figures 2E-F).
163 Taken together, these data suggest that neither the mRNA degradation nor the
164 concurrent transcriptional repression observed during early apoptosis are a
165 consequence of caspase activation.

166 ***Cytoplasmic 3'- but not 5'-RNA exonucleases are required for apoptotic RNAPII***
167 ***transcriptional repression***

168 Based on connections between virus-activated mRNA decay and RNAPII
169 transcription (Abernathy et al., 2015; Gilbertson et al., 2018), we hypothesized that
170 TRAIL-induced mRNA turnover was functionally linked to the concurrent transcriptional
171 repression. Apoptotic mRNA decay occurs from the 3' end by the actions of the
172 cytoplasmic 3'-RNA exonuclease DIS3L2 and the mitochondrial 3'-RNA exonuclease
173 PNPT1, which is released into the cytoplasm by MOMP (Liu et al., 2018; Thomas et al.,
174 2015). This stands in contrast to basal mRNA decay, which occurs predominantly from
175 the 5' end by XRN1 (Jones et al., 2012). We therefore set out determine if 3' or 5' decay
176 factors were required for apoptosis-linked mRNA decay and the ensuing repression of
177 mRNA transcription. Given the likely redundant nature of the multiple 3' end decay
178 factors (Houseley and Tollervey, 2009), we performed concurrent knockdowns of
179 DIS3L2, the RNA exosome component EXOSC4, and PNPT1. To check the
180 involvement of 5' decay, we also depleted the single cytoplasmic 5'-3' exonuclease
181 XRN1 (Figure 3A). Depletion of the 3'-5' but not the 5'-3' decay machinery increased
182 total RNA levels and largely restored RNAPII transcription (Figure 3B-3C). Importantly,
183 there was only a minor reduction in CASP3 activation in cells depleted of 3'-5' decay
184 factors and this was not significantly different from that observed upon XRN1
185 knockdown (Figure 3A). These observations suggest that decreased RNAPII
186 transcription occurs as a consequence of accelerated cytoplasmic mRNA degradation
187 during early apoptosis.

188 ***Apoptosis causes reduced RNAPII promoter occupancy in an mRNA decay-***
189 ***dependent manner***

190 RNAPII is recruited to promoters in an unphosphorylated state, but its
191 subsequent promoter escape and elongation are governed by a series of
192 phosphorylation events in the heptad $(Y_1S_2P_3T_4S_5P_6S_7)_n$ repeats of the RPB1 C-terminal
193 domain (CTD). To determine the stage of transcription impacted by mRNA decay, we
194 performed RNAPII ChIP-qPCR and western blots using antibodies recognizing the
195 different RNAPII phosphorylation states. Occupancy of hypophosphorylated RNAPII at
196 the *ACTB* and *GAPDH* promoters was significantly reduced after 2 hr TRAIL treatment
197 (Figure 3D). In accordance with the 4sU labeling results, siRNA-mediated knockdowns
198 showed that loss of RNAPII occupancy requires cytoplasmic 3'-5' RNA decay factors
199 but not the 5'-3' exonuclease XRN1 (Figure 3D). Impaired binding of the TATA-binding
200 protein (TBP), which nucleates the formation of the RNAPII pre-initiation complex (PIC)
201 at promoters (Buratowski et al., 1989; Louder et al., 2016), mirrored that of RNAPII
202 (Figure 3E). These changes are not driven by alterations in the stability of RPB1 or
203 TBP, since the expression of these proteins remained relatively constant during early
204 apoptosis regardless of the presence of mRNA decay factors (Figure S3A-B). The
205 relative proportion of initiating RPB1 CTD phosphorylated at the serine 5 position and
206 the ratio of serine 5 to serine 2 phosphorylation, which decreases during transcriptional
207 elongation (Shandilya and Roberts, 2012), also remain unchanged during early
208 apoptosis regardless of the presence of mRNA decay factors (Figure 3F). Taken
209 together, these data suggest that the decay-dependent reduction in mRNA synthesis

210 occurs at or before PIC formation, rather than during transcriptional initiation and
211 elongation.

212 ***PABPC1 translocates into the nucleus coincidentally with apoptotic mRNA decay***

213 Virus-induced mRNA decay causes changes in the nucleocytoplasmic
214 localization numerous proteins, the most abundant classes of which are RNA binding
215 proteins (RBPs) that bind the 3' untranslated regions (UTRs) and poly(A) tails of mRNA
216 (Gilbertson et al., 2018). The nuclear accumulation of one such RBP, PABPC1, has
217 been linked to viral endonuclease-induced restrictions of gene expression (Gilbertson et
218 al., 2018; Kumar and Glaunsinger, 2010). We therefore considered the redistribution of
219 RBPs such as PABPC1 as a potential mechanism by which cytoplasmic mRNA decay is
220 sensed by the RNAPII transcriptional machinery in the nucleus.

221 In order to probe whether a redistribution of RBPs similar to that observed during
222 viral nuclease expression occurs during early apoptosis, we performed cell
223 fractionations of apoptotic HCT116 cells. Indeed, 2 hr after TRAIL treatment, PABPC1
224 protein levels increased in the nuclear fraction of cells but not in the cytoplasmic
225 fraction, indicative of relocalization (Figure 4A). This increase in nuclear PABPC was
226 dependent on the presence of CASP8 but not CASP3 (Figure 4A), mirroring the
227 incidence of mRNA decay and reduced RNAPII transcription. Thus, similar to viral
228 infection, PABPC1 relocalization occurs coincidentally with increased mRNA decay and
229 transcriptional repression in the context of early apoptosis.

230 We next tested the hypothesis that PABPC1 participates in the coordination
231 between mRNA decay and transcription by depleting cells of PABPC1 and its functional
232 homolog PABPC4 using siRNAs (Figure S3A). mRNA transcription after 2 hr TRAIL

233 treatment was rescued in PABPC1/4 knock downs (Figure S3B), but baseline mRNA
234 levels in the absence of these proteins were generally greatly reduced (Figure S3C).
235 This is likely consistent with the observation RNAPII promoter occupancy is greatly
236 reduced in the absence of PABPC1/4 (Gilbertson et al., 2018). Thus, depletion of
237 PABPC impairs transcriptional repression during early apoptosis, although given its
238 multiple functions in gene expression (Bernstein et al., 1989; Brook and Gray, 2012;
239 Goss and Kleiman, 2013; Ivanov et al., 2016; Tarun et al., 1997; Wang et al., 1999), the
240 role of PABPC in this process could be indirect.

241 ***Importin α/β transport links mRNA decay and transcription***

242 We next sought to more directly evaluate the role of protein shuttling in
243 connecting cytoplasmic mRNA decay to transcriptional repression. The majority of
244 proteins ~60 kilodaltons (kDa) and larger cannot passively diffuse through nuclear
245 pores; they require assistance by importins to enter the nucleus from the cytoplasm
246 (Gö, 1998). Classical nuclear transport occurs by importin α binding to a cytoplasmic
247 substrate, which is then bound by an importin β to form a tertiary complex that is able to
248 move through nuclear pore complexes (Stewart, 2007). To test if this mode of nuclear
249 transport is required for transcriptional feedback, HCT116 cells were pretreated with
250 ivermectin, a specific inhibitor of importin α/β transport (Wagstaff et al., 2012), before
251 the 2 hr TRAIL treatment. The efficacy of ivermectin was validated by an observed
252 decrease in the nuclear levels of nucleolin (NCL), a known importin α/β substrate
253 (Figure 4B; Kimura et al., 2013). Ivermectin treatment rescued RNAPII transcription
254 (Figure 4C), suggesting that protein trafficking to the nucleus provides signals
255 connecting cytoplasmic mRNA decay to transcription.

256 Importantly, ivermectin did not diminish the extent of CASP3 cleavage (Figure
257 4B) or mRNA decay (Figure S4D) that occurs during early apoptosis, nor did it decrease
258 baseline levels of transcription in non-apoptotic cells (Figure S4E). Interestingly, it also
259 did not prevent PABPC import (Figure 4B), suggesting that PABPC translocation likely
260 occurs via an importin α/β-independent pathway and is necessary but not sufficient to
261 cause repression of RNAPII transcription.

262 Finally, we evaluated whether importin α/β transport is also required for feedback
263 between viral nuclease-driven mRNA decay and RNAPII transcription, as this would
264 suggest that the underlying mechanisms involved in activating this pathway are
265 conserved. We used the mRNA specific endonuclease muSOX from the
266 gammaherpesvirus MHV68, as muSOX expression has been shown to cause
267 widespread mRNA decay and subsequent transcriptional repression (Abernathy et al.,
268 2015, 2014). HEK-293T cell lines were engineered to stably express a dox-inducible
269 wild-type or a catalytically inactive (D219A; Abernathy et al., 2015) form of muSOX.
270 These cells were treated with ivermectin and the resultant changes in RNAPII promoter
271 occupancy were measured by ChIP-qPCR. As expected, expression of WT but not
272 D219A muSOX caused mRNA decay and transcriptional repression (Figs 4D-E, S4F-
273 G). Notably, inhibiting nuclear import with ivermectin (Figure S4F) rescued RNAPII
274 promoter occupancy (Figure 4E) without altering the extent of mRNA decay in muSOX
275 expressing cells (Figure 4D). Thus, importin α/β nuclear transport plays a key role in
276 linking cytoplasmic mRNA decay to nuclear transcription, both during early apoptosis
277 and upon viral nuclease expression.

278 **DISCUSSION**

279 mRNA decay and synthesis rates are tightly regulated in order to maintain
280 appropriate levels of cellular mRNA transcripts (Braun and Young, 2014). It is well
281 established that when cytoplasmic mRNA is stabilized, for example by the depletion of
282 RNA exonucleases, transcription often slows in order to compensate for increased
283 transcript abundance (Haimovich et al., 2013; Helenius et al., 2011; Singh et al., 2019;
284 Sun et al., 2012). Eukaryotic cells thus have the capacity to "buffer" against reductions
285 in mRNA turnover or synthesis. Here, we revealed that a buffering response does not
286 occur under conditions of elevated cytoplasmic mRNA degradation stimulated during
287 early apoptosis. Instead, cells respond to cytoplasmic mRNA depletion by decreasing
288 RNAPII promoter occupancy and transcript synthesis, thereby amplifying the magnitude
289 of the gene expression shut down. Nuclear import of cytoplasmic proteins is required for
290 this "transcriptional feedback", suggesting a pathway of gene regulation in which
291 enhanced mRNA decay prompts cytoplasmic proteins to enter the nucleus and halt
292 mRNA production. Notably, similar transcriptional feedback is elicited during virus-
293 induced mRNA decay (Abernathy et al., 2015; Gilbertson et al., 2018; Hartenian et al.,
294 2020), indicating that distinct cellular stresses can converge on this pathway to
295 potentiate a multi-tiered shutdown of gene expression.
296 Multiple experiments support the conclusion that the TRAIL-induced
297 transcriptional repression phenotype is a consequence cytoplasmic decay triggered by
298 MOMP, rather than caspase activity. XRN1-driven 5'-3' end decay is the major pathway
299 involved in basal mRNA decay (Łabno et al., 2016), but MOMP-induced mRNA decay is
300 primarily driven by 3' exonucleases such as PNPT1 and DIS3L2 (Liu et al., 2018;
301 Thomas et al., 2015). Accordingly, co-depletion of 3' decay factors but not XRN1

302 restored RNAPII promoter occupancy and transcription during early apoptosis. In
303 contrast to that of 3' mRNA decay factors, depletion of CASP3 (or the caspase activated
304 DNase CAD) did not block mRNA degradation or transcriptional repression, even
305 though CASP3 is responsible for the vast majority of proteolysis that is characteristic of
306 apoptotic cell death (Walsh et al., 2008). Additionally, the initiator CASP8 was required
307 only under conditions where its activity was needed to induce MOMP. These findings
308 reinforce the idea that mRNA decay and transcriptional repression are very early events
309 that are independent of the subsequent cascade of caspase-driven phenotypes
310 underlying many of the hallmark features of apoptosis.

311 A key open question is what signal conveys cytoplasmic mRNA degradation
312 information to the nucleus to cause transcriptional repression. Our data support a model
313 where the signal during early apoptosis is provided by one or more proteins that are
314 imported into the nucleus in response to accelerated mRNA decay, rather than
315 depletion of transcriptional machinery. Indeed, many RNA binding proteins undergo
316 nuclear-cytoplasmic redistribution under conditions of viral nuclease-induced mRNA
317 decay, including PABPC (Gilbertson et al., 2018; Kumar et al., 2011; Kumar and
318 Glaunsinger, 2010). We propose that a certain threshold of mRNA degradation is
319 necessary to elicit protein trafficking and transcriptional repression. Presumably, normal
320 levels of basal mRNA decay and regular cytoplasmic repopulation result in a balanced
321 level of mRNA-bound versus unbound proteins. However, if this balance is tipped during
322 accelerated mRNA decay, an excess of unbound RNA binding proteins could
323 accumulate and be transported into the nucleus.

324 PABPC1 is likely among the first proteins released from mRNA transcripts
325 undergoing 3' end degradation, and its nuclear translocation is driven by a poly(A)-
326 masked nuclear localization signal that is exposed upon RNA decay (Kumar et al.,
327 2011). Depletion of PABPC1/4 impairs mRNA decay-driven transcriptional feedback
328 both during apoptosis and upon viral endonuclease expression, suggesting they are a
329 component of this signaling pathway. However, the nuclear accumulation of PABPC1
330 during early apoptosis is not sufficient to induce transcriptional repression and its
331 depletion also negatively impacts mRNA abundance. It is therefore likely that nuclear
332 import of additional proteins via the importin α/β pathway is critical for reduced mRNA
333 production. The requirement for importin α/β–mediated nuclear transport in both
334 apoptosis-induced and viral nuclease-induced transcriptional repression suggests that
335 these two stimuli activate a conserved pathway of gene regulation. Whether other types
336 of cell stress elicit a similar response remains an important question for future
337 investigation.
338 The mRNA 3' end decay-dependent decrease in RNA synthesis is accompanied
339 by a reduction in TBP and RNAPII occupancy at promoters, consistent with
340 transcriptional inhibition occurring upstream of RNAPII initiation and elongation
341 (Gilbertson et al., 2018; Hartenian et al., 2020). The mechanism driving such a defect is
342 yet to be defined, but possibilities include changes to transcript processing pathways,
343 transcriptional regulators, or the chromatin state that directly or indirectly impact
344 formation of the preinitiation complex. In this regard, mRNA processing and
345 transcription are functionally linked (Bentley, 2014) and nuclear accumulation of
346 PABPC1 has been shown to affect mRNA processing by inducing hyperadenylation of

347 nascent transcripts (Kumar and Glaunsinger, 2010; Lee and Glaunsinger, 2009).
348 Furthermore, TBP interacts with the cleavage–polyadenylation specificity factor
349 (Dantonel et al., 1997), providing a possible link between RNAPII preinitiation complex
350 assembly and polyadenylation. Such a mechanism could also explain the specificity of
351 the observed transcriptional repression to RNAPII transcripts. Chromatin architecture
352 could also be influenced by shuttling of RNA binding proteins, as for example the yeast
353 nucleocytoplasmic protein Mrn1 is implicated in the function of chromatin remodeling
354 complexes (Düring et al., 2012). Future work will test these possibilities in order to
355 mechanistically define the connection between nuclear import and RNAPII transcription
356 under conditions of enhanced mRNA decay.

357 There are several potential benefits to dampening mRNA transcription in
358 response to accelerated mRNA turnover. Debris from apoptotic cells is usually cleared
359 by macrophages, but inefficient clearance of dead cells can lead to the development of
360 autoantibodies to intracellular components such as histones, DNA, and
361 ribonucleoprotein complexes. This contributes to autoimmune conditions such as
362 systemic lupus erythematosus (Caruso and Poon, 2018; Nagata et al., 2010). In the
363 context of infection, many viruses require the host RNAPII transcriptional machinery to
364 express viral genes (Harwig et al., 2017; Rivas et al., 2016; Walker and Fodor, 2019). It
365 may therefore be advantageous for the cell to halt transcription in attempt to pre-empt a
366 viral takeover of mRNA synthesis. That said, as with antiviral translational shutdown
367 mechanisms (Walsh et al., 2013), viruses have evolved strategies to evade
368 transcriptional repression (Hartenian et al., 2020; Harwig et al., 2017), as well as inhibit
369 cell death via apoptosis and/or co-opt apoptotic signaling cascades (Suffert et al., 2011;

370 Tabtieng et al., 2018; Zhang et al., 2013; Zhou et al., 2017). In either case, the
371 shutdown of transcription in a cell under stress may protect surrounding cells from
372 danger, particularly in an in vivo context. If true, this type of response is likely to be
373 more relevant in multicellular compared with unicellular organisms.

374 **ACKNOWLEDGEMENTS**

375 This work was supported by NIH grant R01CA136367 to B.G. and the HHMI Gilliam
376 Fellowship for Advanced Study to C.D. B.G. is an investigator of the Howard Hughes
377 Medical Institute. We thank the UC Berkeley Cell Culture Facility for providing the cell
378 lines used in this study, in addition to the UC Berkeley DNA Sequencing Facility and all
379 members of the Glaunsinger and Coscoy labs for providing valuable feedback.

380 **AUTHOR CONTRIBUTIONS**

381 C.D. conceived and performed the experiments, analyzed and visualized the data,
382 acquired funding, and drafted the manuscript. E.H. created the stable cell lines and
383 drafted the corresponding section of the manuscript. B.G. conceived and supervised the
384 study, acquired funding, and edited the manuscript.

385 **DECLARATION OF INTERESTS**

386 The authors declare no competing interests.

387

388

389

390

391

392

FIGURE 1

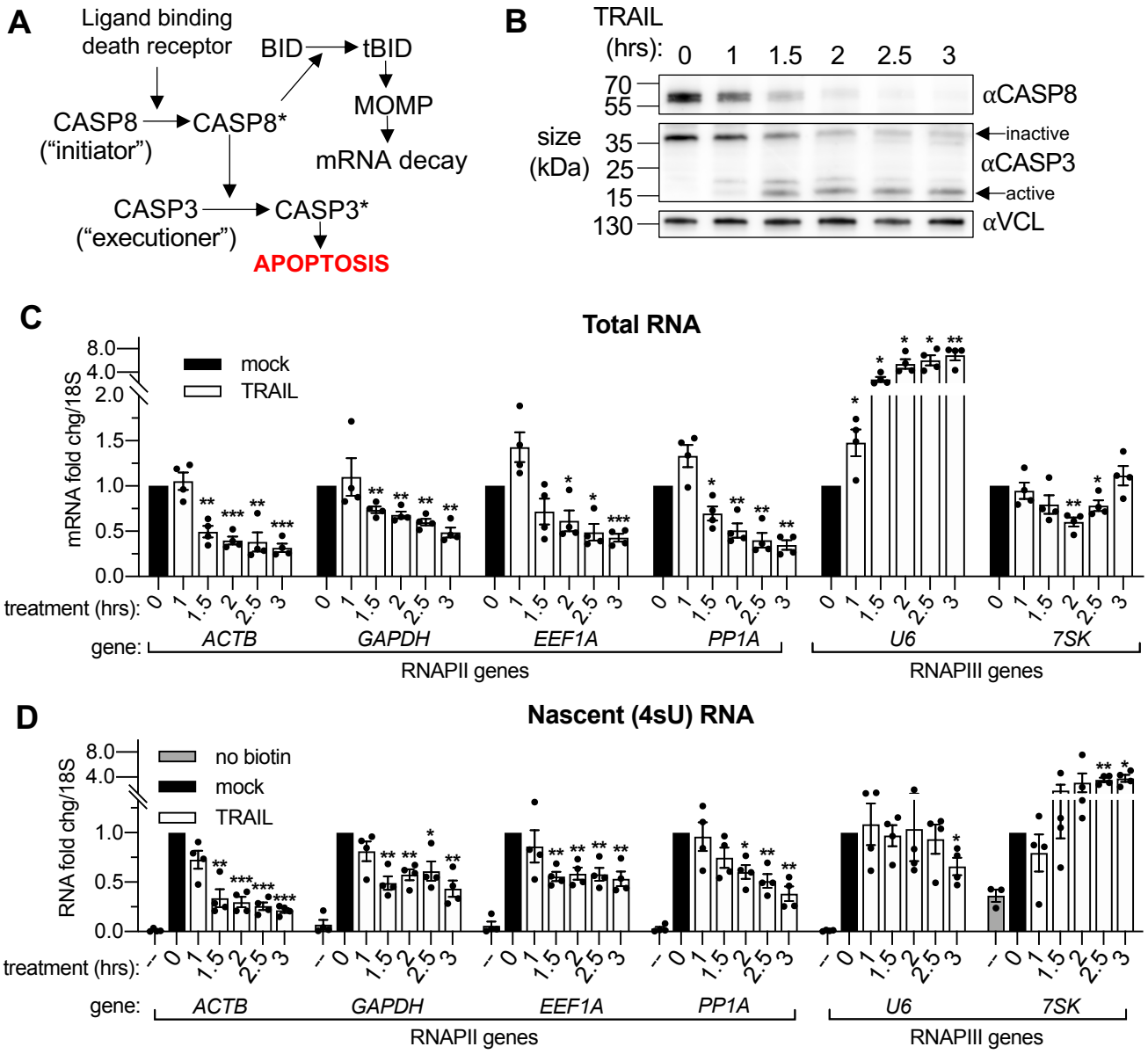
A
Ligand binding death receptor
BID
tBID
CASP8 ("initiator")
CASP8*
MOMP
mRNA decay
CASP3 ("executioner")
CASP3*
APOPTOSIS
B
TRAIL (hrs): 0 1 1.5 2 2.5 3
size (kDa)
70
55
35
25
15
130
αCASP8
inactive
αCASP3
active
αVCL
C
Total RNA
mRNA fold chg/18S
mock
TRAIL
treatment (hrs): 0 1 1.5 2 2.5 3
gene: ACTB GAPDH EEF1A PP1A U6 7SK
RNAPII genes
RNAPIII genes
D
Nascent (4sU) RNA
RNA fold chg/18S
no biotin
mock
TRAIL
treatment (hrs): – 0 1 1.5 2 2.5 3
gene: ACTB GAPDH EEF1A PP1A U6 7SK
RNAPII genes
RNAPIII genes

393 **Figure 1.** mRNA decay during early apoptosis is accompanied by reduced synthesis of
394 RNAPII transcripts. (A) Schematic representation of how the extrinsic apoptotic pathway
395 accelerates mRNA decay. (B) Western blot of HCT116 lysates showing caspase 8
396 (CASP8) and caspase 3 (CASP3) cleavage and activation over a time course of 100
397 ng/μL TRAIL treatment. Vinculin (VCL) serves as a loading control. (C, D) RT-qPCR
398 quantification of total (C) and nascent 4sU pulse-labeled (D) RNA at the indicated times
399 post TRAIL treatment of HCT116 cells. Also see Figure S1. No biotin control quantifies
400 RNA not conjugated to biotin that is pulled down with strepdavidin selection beads. Fold
401 changes were calculated from Ct values normalized to *18S* rRNA in reference to mock
402 treated cells. Graphs display mean +/- SEM with individual biological replicates
403 represented as dots. Statistically significant deviation from a null hypothesis of 1 was
404 determined using one sample t test; *$p<0.05$, **$p<0.01$, ***$p<0.001$.
405
406
407
408
409
410
411
412
413
414

FIGURE 2

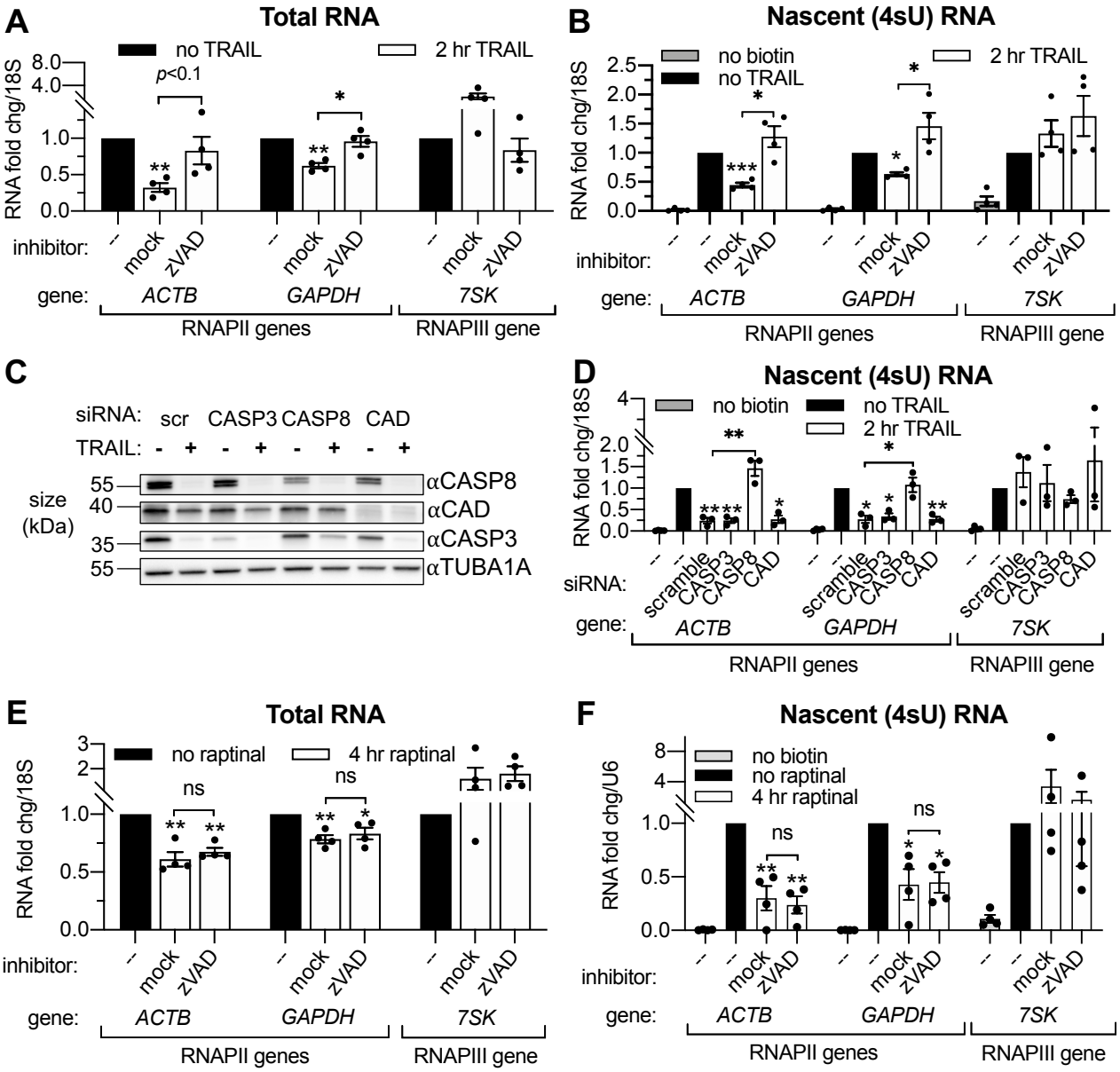
A
Total RNA
no TRAIL
2 hr TRAIL
p<0.1
RNA fold chg/18S
inhibitor:
mock
zVAD
gene:
ACTB
GAPDH
7SK
RNAPII genes
RNAPIII gene
B
Nascent (4sU) RNA
no biotin
no TRAIL
2 hr TRAIL
C
siRNA:
scr
CASP3
CASP8
CAD
TRAIL:
size (kDa)
αCASP8
αCAD
αCASP3
αTUBA1A
D
Nascent (4sU) RNA
no biotin
no TRAIL
2 hr TRAIL
scramble
E
Total RNA
no raptinal
4 hr raptinal
ns
F
Nascent (4sU) RNA
no biotin
no raptinal
4 hr raptinal
RNA fold chg/U6

415 **Figure 2**. Transcriptional repression during early apoptosis requires MOMP but is not
416 directly dependent on caspase activity. (A, B) RT-qPCR measurements of total (A) and
417 nascent 4sU-labeled (B) RNA fold changes after 2 hr TRAIL treatment of HCT116 cells,
418 including a 1 hr pre-treatment with either 40 μM zVAD or an equal volume of DMSO
419 ("mock"). Also see Figure S2A. (C) Western blots showing the efficiency of CASP3,
420 CASP8, and caspase-activated DNase (CAD) protein depletion following treatment with
421 the indicated siRNAs. α-Tubulin (TUBA1A) serves as a loading control. (D) RT-qPCR
422 measurements of 4sU-labeled nascent transcripts before or after 2 hr TRAIL treatment
423 in the siRNA treated samples shown in (*C*). Also see Figures S2B-E. (E, F) Total (E)
424 and nascent 4sU-labeled (F) RNA levels measured by RT-qPCR in HeLa cells after 10
425 μM raptinal treatment for 4 hr, with or without a 1 hr pre-treatment of 20 μM zVAD. Also
426 see Figure S2F. RNA Fold changes were calculated from Ct values normalized to *18S*
427 or *U6* RNA then normalized to non-apoptotic cells under otherwise identical conditions.
428 Graphs display mean +/- SEM with individual biological replicates represented as dots.
429 Statistically significant deviation from a null hypothesis of 1 was determined using one
430 sample t test and indicated with asterisks directly above bars, while multiple t tests with
431 the Holm-Sidak correction for multiple comparisons were performed to compare mean
432 fold change values for mock inhibitor or scramble siRNA-treated cells to those treated
433 with zVAD or a targeting siRNA and indicated with brackets. *p<0.05, **p<0.0.1,
434 ***p<0.001.
435
436

FIGURE 3

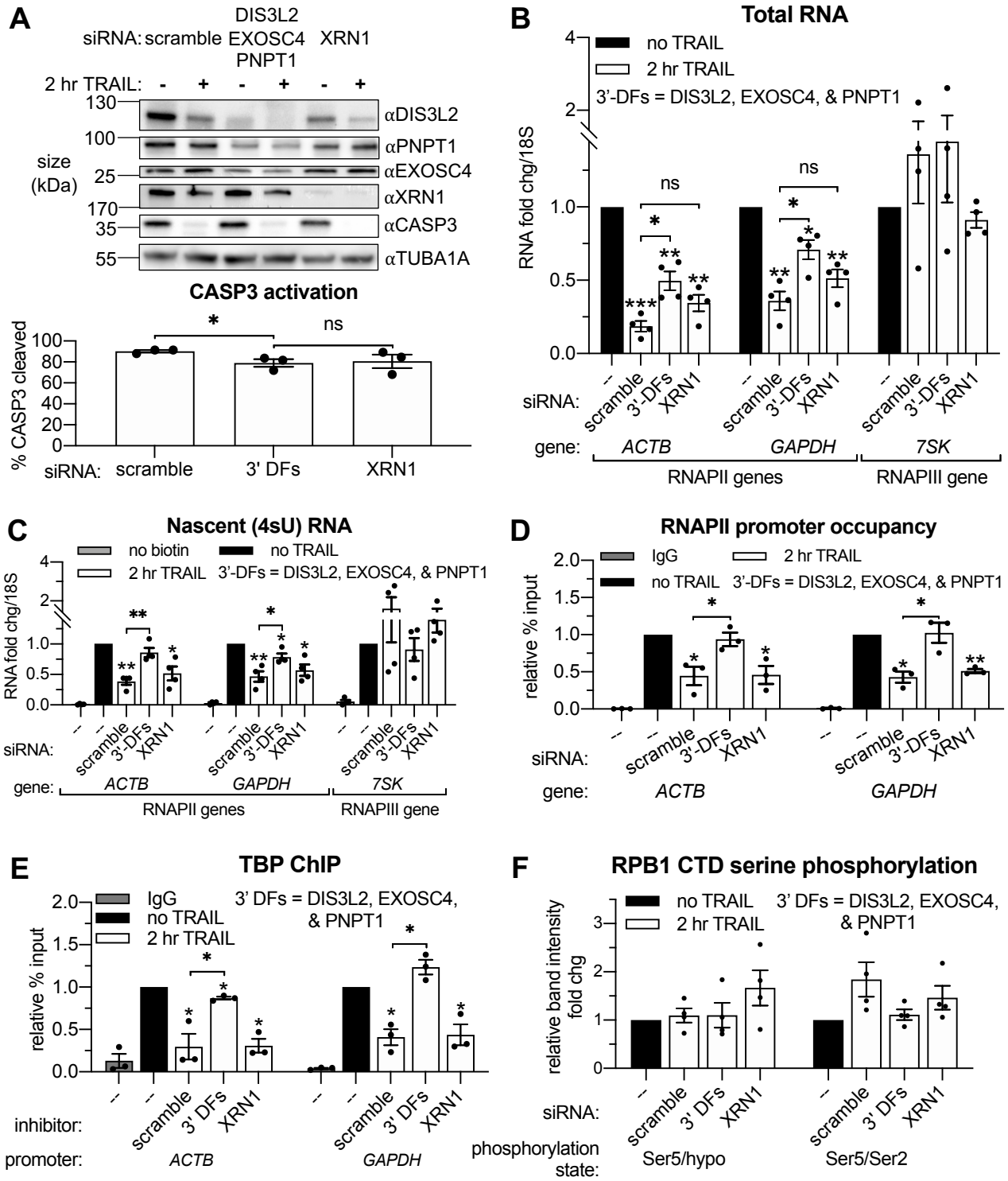
A
DIS3L2
siRNA: scramble EXOSC4 XRN1
PNPT1
2 hr TRAIL: - + - + - +
130
100
25
170
35
55
size (kDa)
αDIS3L2
αPNPT1
αEXOSC4
αXRN1
αCASP3
αTUBA1A
CASP3 activation
% CASP3 cleaved
siRNA: scramble 3' DFs XRN1
B
Total RNA
no TRAIL
2 hr TRAIL
3'-DFs = DIS3L2, EXOSC4, & PNPT1
RNA fold chg/18S
siRNA:
gene: ACTB GAPDH 7SK
RNAPII genes
RNAPIII gene
C
Nascent (4sU) RNA
no biotin
no TRAIL
2 hr TRAIL
3'-DFs = DIS3L2, EXOSC4, & PNPT1
RNA fold chg/18S
siRNA:
gene: ACTB GAPDH 7SK
RNAPII genes
RNAPIII gene
D
RNAPII promoter occupancy
IgG
2 hr TRAIL
no TRAIL
3'-DFs = DIS3L2, EXOSC4, & PNPT1
relative % input
siRNA:
gene: ACTB GAPDH
E
TBP ChIP
IgG
no TRAIL
2 hr TRAIL
3' DFs = DIS3L2, EXOSC4, & PNPT1
relative % input
inhibitor:
promoter: ACTB GAPDH
F
RPB1 CTD serine phosphorylation
no TRAIL
2 hr TRAIL
3' DFs = DIS3L2, EXOSC4, & PNPT1
relative band intensity fold chg
siRNA:
phosphorylation state: Ser5/hypo Ser5/Ser2

437 **Figure 3.** Apoptosis causes reduced RNAPII transcriptional output and promoter
438 occupancy in an mRNA decay-dependent manner. (A) Western blots of lysates of
439 HCT116 cells depleted of the indicated decay factors with and without 2 hr TRAIL
440 treatment. Apoptosis induction was confirmed by disappearance of the full-length
441 CASP3 band, quantified in the graph below by measuring band intensity normalized to
442 an α-tubulin (TUBA1A) loading control. (B, C) Total (B) and nascent 4sU-labeled (*C*)
443 RNA was quantified by RT-qPCR under the cellular conditions described in (A). Fold
444 changes were calculated from Ct values normalized to *18S* rRNA. (D, E) Chromatin
445 immunoprecipitation (ChIP)-qPCR was used to measure occupancy of the indicated
446 promoters by hypophosorylated RNAPII (D) or TBP (E) under cellular conditions
447 described in (A). Rabbit and mouse IgG antibodies were included in parallel
448 immunoprecipitation reactions with chromatin from scramble siRNA-treated non-
449 apoptotic cells in lieu of TBP and RNAPII antibodies, respectively, as a control. Also see
450 Figures S3A-B, (F) Relative band intensity ratios from 4 replicates of the representative
451 western blots depicted in S3A, using primary antibodies specific to the indicated RPB1
452 CTD phosphorylation state under cellular conditions described in (A). Band intensity
453 values were first normalized to a vinculin (VCL) loading control in each blot. All bar
454 graphs display mean +/- SEM with individual biological replicates represented as dots.
455 Statistically significant deviation from a null hypothesis of 1 was determined using one
456 sample t test and indicated with asterisks directly above bars, while multiple t tests with
457 the Holm-Sidak correction for multiple comparisons were performed to compare mean
458 values between groups indicated with brackets. $^{*}p<0.05$, $^{**}p<0.0.1$, $^{***}p<0.001$.

FIGURE 4

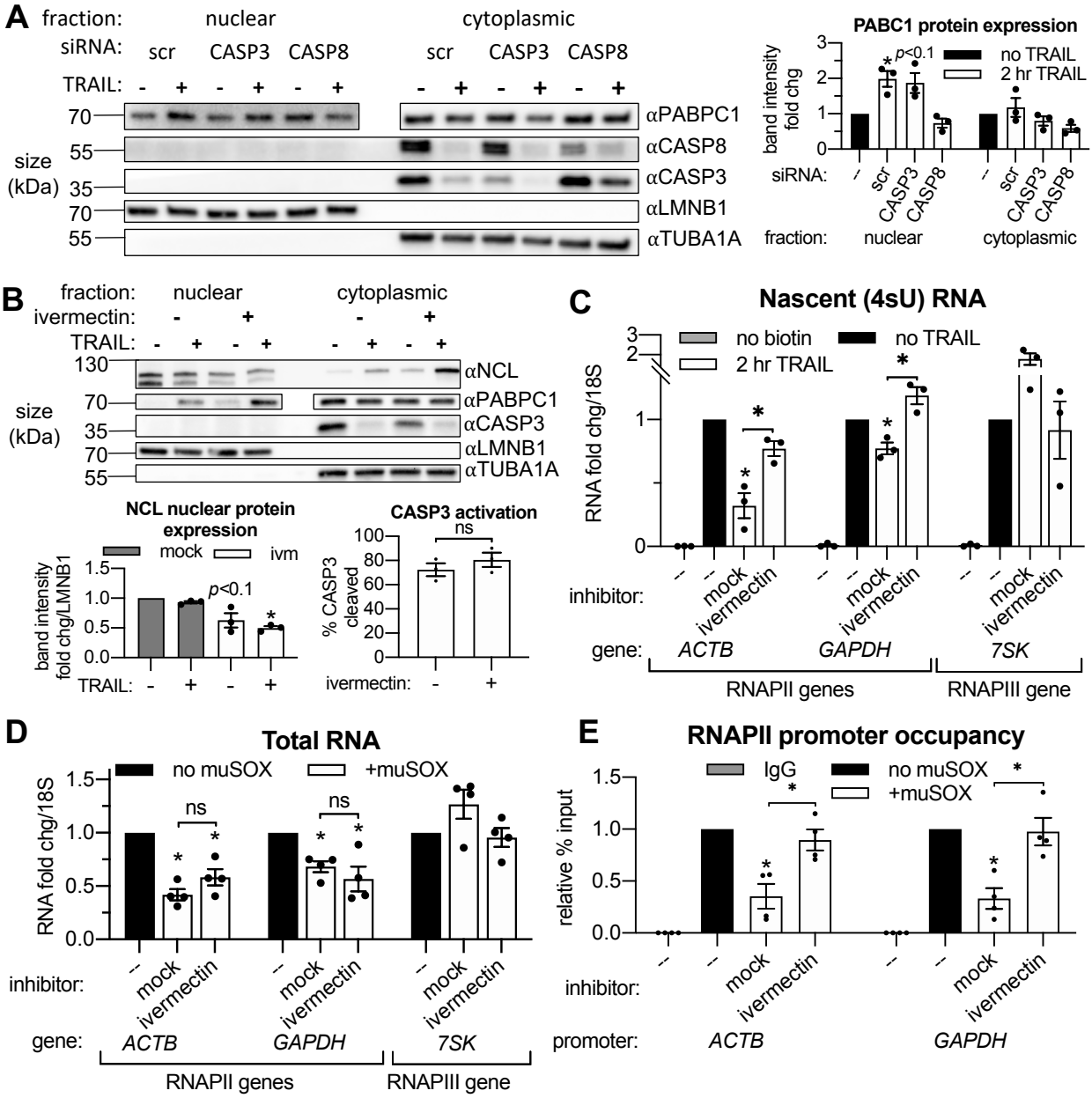
A
fraction: nuclear cytoplasmic
siRNA: scr CASP3 CASP8 scr CASP3 CASP8
TRAIL: - + - + - + - + - + - +
size (kDa)
70 55 35 70 55
αPABPC1
αCASP8
αCASP3
αLMNB1
αTUBA1A
PABC1 protein expression
band intensity fold chg
p<0.1
no TRAIL
2 hr TRAIL
siRNA: / scr CASP3 CASP8 / scr CASP3 CASP8
fraction: nuclear cytoplasmic
B
fraction: nuclear cytoplasmic
ivermectin: - + - +
TRAIL: - + - + - + - +
130 70 35 70 55
αNCL
αPABPC1
αCASP3
αLMNB1
αTUBA1A
NCL nuclear protein expression
mock ivm
band intensity fold chg/LMNB1
p<0.1
TRAIL: - + - +
CASP3 activation
% CASP3 cleaved
ns
ivermectin: - +
C
Nascent (4sU) RNA
no biotin
no TRAIL
2 hr TRAIL
RNA fold chg/18S
inhibitor: -- -- mock ivermectin -- -- mock ivermectin -- -- mock ivermectin
gene: ACTB GAPDH 7SK
RNAPII genes
RNAPIII gene
D
Total RNA
no muSOX
+muSOX
RNA fold chg/18S
ns
inhibitor: -- mock ivermectin -- mock ivermectin -- mock ivermectin
gene: ACTB GAPDH 7SK
RNAPII genes
RNAPIII gene
E
RNAPII promoter occupancy
IgG
no muSOX
+muSOX
relative % input
inhibitor: -- -- mock ivermectin -- -- mock ivermectin
promoter: ACTB GAPDH

459 **Figure 4.** Importin α/β transport links mRNA decay and transcription. (A) Western blots
460 showing the indicated proteins in the nuclear and cytoplasmic fractions of apoptotic and
461 non-apoptotic HCT116 cells nucleofected with scramble, CASP3, or CASP8 siRNAs.
462 The nuclear and cytoplasmic fractions of PABPC1 were imaged together but cropped
463 and edited separately to account for the large disparity between the nuclear and
464 cytoplasmic band intensities for this traditionally cytoplasmic protein. The graph on the
465 right shows the changes in PABPC1 abundance in the nucleus versus cytoplasm in the
466 indicated siRNA treated samples. Protein abundance was calculated by band intensity
467 in reference to lamin B1 (LMNB1) or α-tubulin (TUBA1A) loading controls, for the
468 nuclear and cytoplasmic fractions, respectively. Also see Figures S4A-C. (B) Nuclear
469 and cytoplasmic expression of the indicated proteins in apoptotic and non-apoptotic
470 cells with a 1 hr pre-treatment with 25 μM ivermectin or an equal volume of EtOH
471 ("mock"). Nuclear levels of nucleolin (NCL) were quantified by band intensity in
472 reference to a LMNB1 loading control, while disappearance of full-length CASP3 was
473 quantified in the cytoplasm in reference to TUBA1A. The nuclear and cytoplasmic
474 fractions of PABPC1 were imaged together but cropped and edited separately to
475 account for the large disparity between the nuclear and cytoplasmic band intensities for
476 this traditionally cytoplasmic protein. (C) Levels of nascent 4sU-labeled RNA were
477 quantified by RT-qPCR under the cellular conditions described in (B). Also see Figures
478 S4D-E. (D) RT-qPCR quantification of total RNA levels in HEK293T cells stably
479 expression a doxycycline (dox)-inducible form of muSOX endonuclease cultured with or
480 without 1 μg/mL dox for 48 hr, ending with a 2 hr treatment with 25 μM ivermectin or an
481 equal volume of EtOH. (E) RNAPII promoter occupancy at the *ACTB* and *GAPDH*

482 promoters was determined by ChIP-qPCR under cellular conditions described in (*D*).
483 Also see Figures S2D-G. RNA fold changes were calculated from Ct values normalized
484 to *18S* rRNA. All bar graphs display mean +/- SEM with individual biological replicates
485 represented as dots. Statistically significant deviation from a null hypothesis of 1 was
486 determined using one sample t test and indicated with asterisks directly above bars,
487 while multiple t tests with the Holm-Sidak correction for multiple comparisons were
488 performed to compare mean values between groups indicated with brackets. **p*<0.05,
489 ***p*<0.0.1, ****p*<0.001.
490
491
492
493
494
495
496
497
498
499
500
501
502
503

FIGURE S1

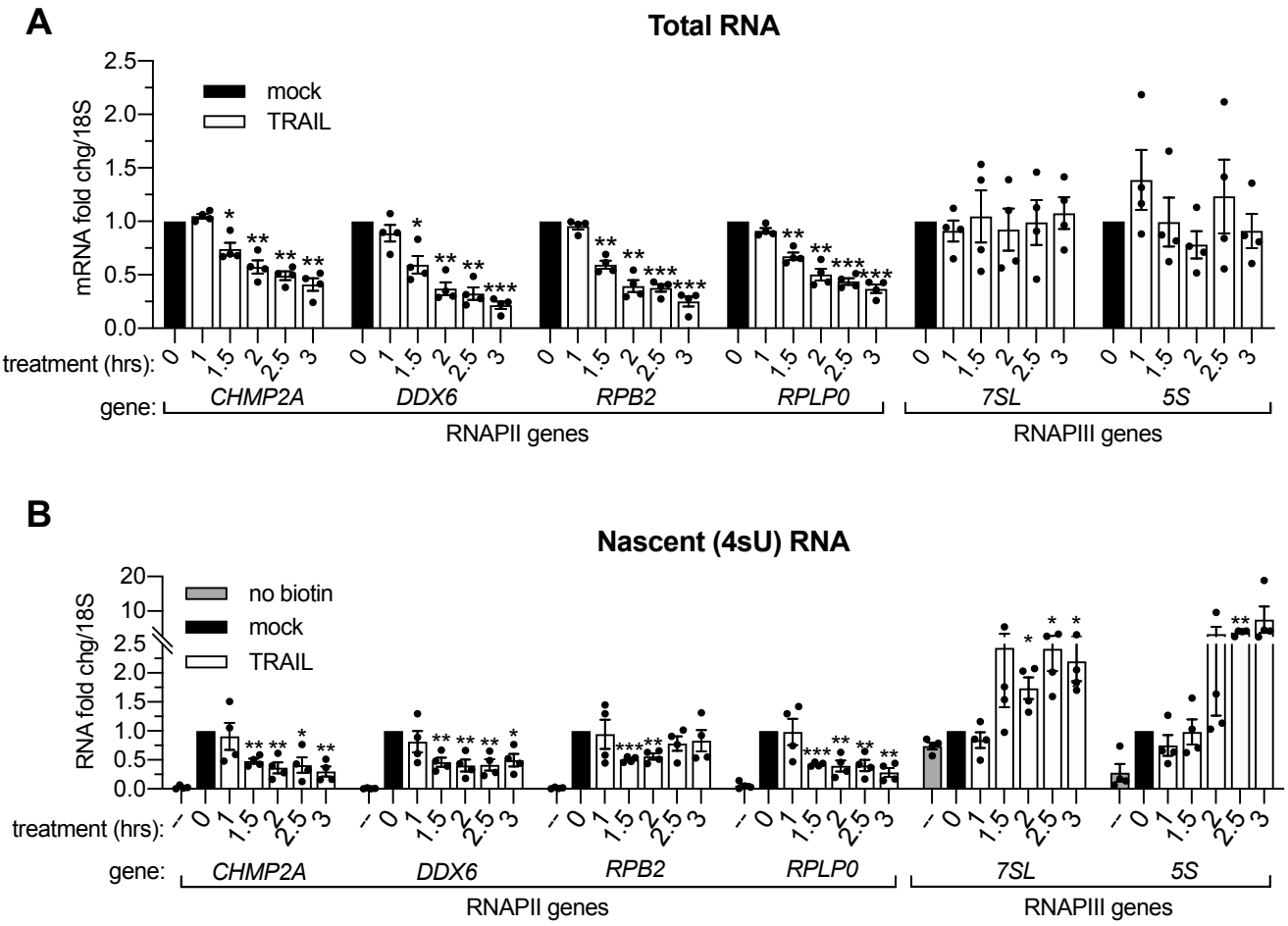
A
Total RNA
mRNA fold chg/18S
mock
TRAIL
treatment (hrs):
gene:
CHMP2A
DDX6
RPB2
RPLP0
7SL
5S
RNAPII genes
RNAPIII genes
B
Nascent (4sU) RNA
RNA fold chg/18S
no biotin
mock
TRAIL
treatment (hrs):
gene:
CHMP2A
DDX6
RPB2
RPLP0
7SL
5S
RNAPII genes
RNAPIII genes

504 **Figure S1.** mRNA decay during early apoptosis is accompanied by reduced synthesis
505 of RNAPII transcripts. (A, B) RT-qPCR quantification of total (C) and nascent 4sU pulse-
506 labeled (D) RNA at the indicated times post TRAIL treatment of HCT116 cells. Fold
507 changes were calculated from Ct values normalized to *18S* rRNA in reference to mock
508 treated cells. Graphs display mean +/- SEM with individual biological replicates
509 represented as dots. Statistically significant deviation from a null hypothesis of 1 was
510 determined using one sample t test; *$p<0.05$, **$p<0.01$, ***$p<0.001$.
511
512
513
514
515
516
517
518
519
520
521
522
523
524
525

FIGURE S2

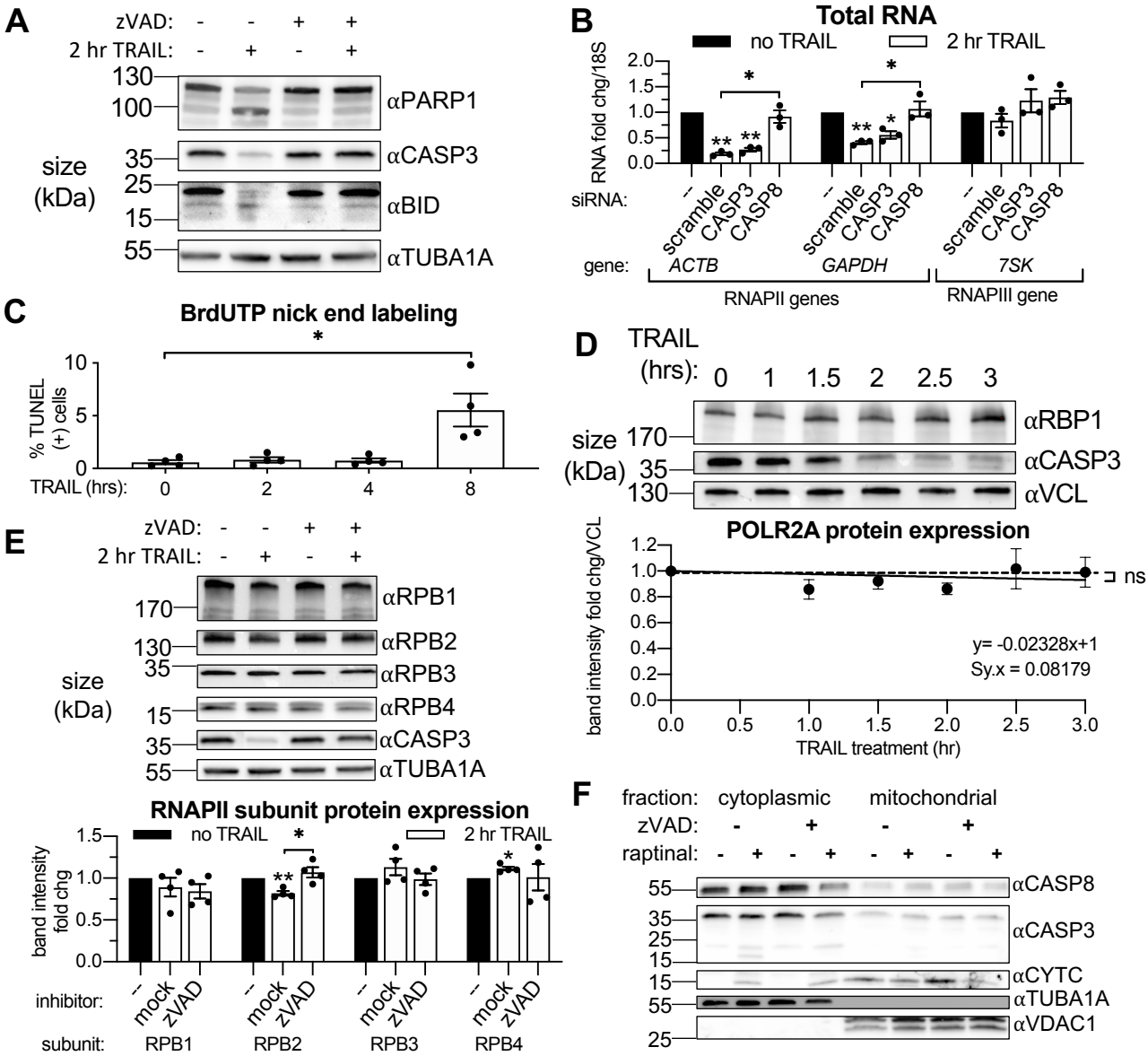
A
zVAD: - - + +
2 hr TRAIL: - + - +
size (kDa)
130
100
35
25
15
55
αPARP1
αCASP3
αBID
αTUBA1A
B
Total RNA
no TRAIL
2 hr TRAIL
RNA fold chg/18S
siRNA:
scramble
CASP3
CASP8
gene:
ACTB
GAPDH
7SK
RNAPII genes
RNAPIII gene
C
BrdUTP nick end labeling
% TUNEL (+) cells
TRAIL (hrs): 0 2 4 8
D
TRAIL (hrs): 0 1 1.5 2 2.5 3
size (kDa)
170
35
130
αRBP1
αCASP3
αVCL
POLR2A protein expression
band intensity fold chg/VCL
ns
y= -0.02328x+1
Sy.x = 0.08179
TRAIL treatment (hr)
E
zVAD: - - + +
2 hr TRAIL: - + - +
size (kDa)
170
130
35
15
35
55
αRPB1
αRPB2
αRPB3
αRPB4
αCASP3
αTUBA1A
RNAPII subunit protein expression
no TRAIL
2 hr TRAIL
band intensity fold chg
inhibitor:
mock
zVAD
subunit:
RPB1
RPB2
RPB3
RPB4
F
fraction: cytoplasmic mitochondrial
zVAD: - + - +
raptinal: - + - + - + - +
55
35
25
15
15
55
25
αCASP8
αCASP3
αCYTC
αTUBA1A
αVDAC1

526 **Figure S2**. Transcriptional repression during early apoptosis requires MOMP but is not
527 dependent on caspase activity. (A) Western blot of HCT116 lysates showing cleavage
528 (or lack thereof) of the caspase 8 (CASP8) targets BID and caspase 3 (CASP3), as well
529 as the CASP3 target PARP1 upon 2 hr 100 ng/μL TRAIL treatment in the presence or
530 absence of 40 μM zVAD. (B) RT-qPCR quantification of the change in total RNA levels
531 in HCT116 cells treated with the indicated siRNAs upon 2 hr TRAIL treatment. Fold
532 change were calculated from Ct values normalized to *18S* rRNA. (C) Quantification of
533 BrdUTP-labeled HCT116 cells treated with TRAIL for the indicated times in a TUNEL
534 assay. Percent positive cells calculated by flow cytometry using FloJo imaging software
535 to count the number of cells with elevated FL2 fluorescence. (D) Western blot of
536 HCT116 lysates showing RPB1 levels and activation over a time course of TRAIL
537 treatment. Vinculin (VCL) serves as a loading control. Graph below quantifies mean
538 RPB1 levels by VCL-normalized band intensity from 4 biological replicates and analyzes
539 the resultant curve by simple linear regression with a set x intercept of 1. These data
540 are derived from the same experiment depicted in Figures 1B-D and S1A-B, therefore
541 the VCL and CASP3 panels are identical to that of Figure 1B. (E) Western blot of
542 HCT116 lysates from cells under conditions described in (A) depicting levels of the
543 indicated RNAPII subunits and CASP3 activation. α-Tubulin (TUBA1A) serves as a
544 loading control. Graph below quantifies the change in RNAPII subunit levels upon
545 apoptosis induction by TUBA1A-normalized band density. (F) Western blots of the
546 cytoplasmic and mitochondrial fractions of HeLa cells treated with 10 μM raptinal or
547 equal volume of DMSO, in the presence of 20 μM zVAD or additional volume of DMSO.
548 Efficacy of raptinal treatment was demonstrated by cytochrome c (CYTC) release into

549 the cytoplasm in the presence and absence of zVAD, which effectively blocked the
550 cleavage and activation of CASP3. TUBA1A and VDAC1 served as cytoplasmic and
551 mitochondrial loading controls, respectively. All bar graphs display mean +/- SEM with
552 individual biological replicates represented as dots. Statistically significant deviation
553 from a null hypothesis of 1 was determined using one sample t test and indicated with
554 asterisks directly above bars, while multiple t tests with the Holm-Sidak correction for
555 multiple comparisons were performed to compare mean values between groups
556 indicated with brackets. *p<0.05, **p<0.0.1, ***p<0.001.
557
558
559
560
561
562
563
564
565
566
567
568
569
570

FIGURE S3

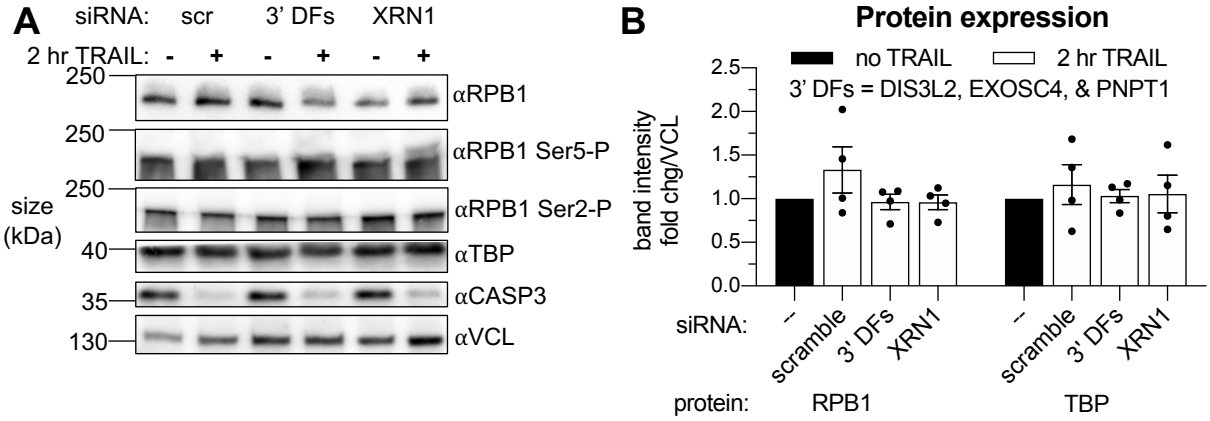
A
siRNA: scr 3' DFs XRN1
2 hr TRAIL: - + - + - +
250
250
250
40
35
130
size (kDa)
αRPB1
αRPB1 Ser5-P
αRPB1 Ser2-P
αTBP
αCASP3
αVCL
B
Protein expression
no TRAIL
2 hr TRAIL
3' DFs = DIS3L2, EXOSC4, & PNPT1
band intensity fold chg/VCL
2.5
2.0
1.5
1.0
0.5
0.0
siRNA:
--
scramble
3' DFs
XRN1
protein:
RPB1
TBP

571 **Figure S3.** Apoptosis causes reduced RNAPII transcriptional output and promoter
572 occupancy in an mRNA decay-dependent manner. (A) Representative western blots on
573 lysates of HCT116 cells depleted of either 3' DFs (DIS3L2, EXOSC4, and PNPT1) or
574 XRN1 before and after 2 hr TRAIL treatment, probing for the indicated protein or RPB1
575 C-terminal domain (CTD) phosphorylation state. Apoptosis induction was confirmed by
576 observing CASP3 cleavage. A vinculin (VCL) loading control was imaged for the blots of
577 each phosphorylation state but a single representative panel is shown. Quantification of
578 RPB1 phosphorylation states from 4 replicates displayed in Figure 3F. (B) Band
579 intensity fold changes of hypophosphorylated RPB1 and TBP derived from 4 biological
580 replicates of the experiment described in (A). Bar graph displays mean +/- SEM with
581 individual biological replicates represented as dots. No statistically significant deviations
582 were discovered either from one-sample t tests of fold change values with a null
583 hypothesis of 1 or multiple t tests with the Holm-Sidak correction for multiple
584 comparisons comparing mean values between siRNA treatments.
585
586
587
588
589
590
591
592

FIGURE S4

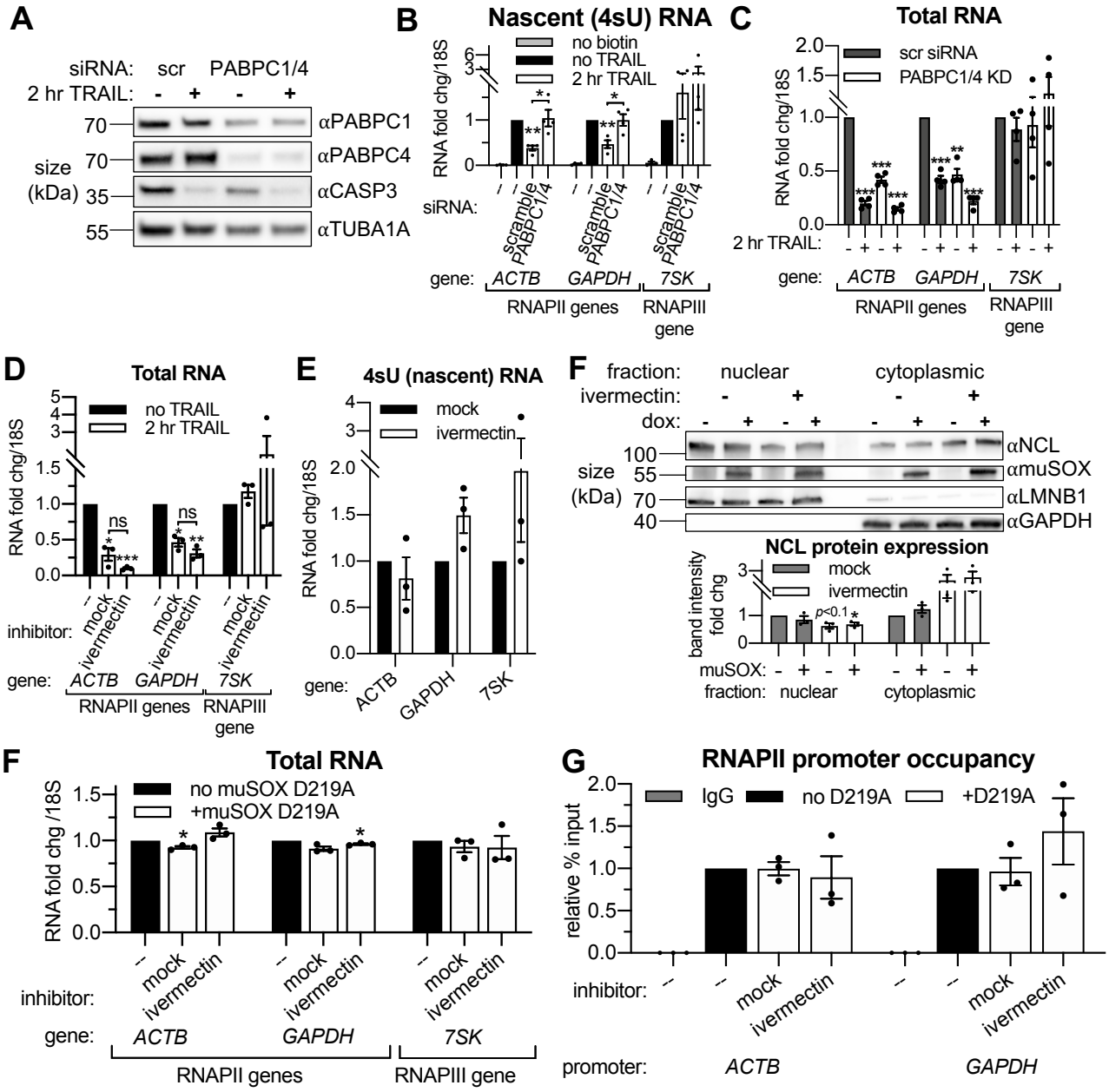
A
siRNA: scr PABPC1/4
2 hr TRAIL: - + - +
70 αPABPC1
70 αPABPC4
size (kDa) 35 αCASP3
55 αTUBA1A
B
Nascent (4sU) RNA
no biotin
no TRAIL
2 hr TRAIL
RNA fold chg/18S
siRNA: scramble PABPC1/4
gene: ACTB GAPDH 7SK
RNAPII genes
RNAPIII gene
C
Total RNA
scr siRNA
PABPC1/4 KD
RNA fold chg/18S
2 hr TRAIL: - + - + - + - + - + - +
gene: ACTB GAPDH 7SK
RNAPII genes
RNAPIII gene
D
Total RNA
no TRAIL
2 hr TRAIL
RNA fold chg/18S
ns
inhibitor: – mock ivermectin
gene: ACTB GAPDH 7SK
RNAPII genes
RNAPIII gene
E
4sU (nascent) RNA
mock
ivermectin
RNA fold chg/18S
gene: ACTB GAPDH 7SK
F
fraction: nuclear cytoplasmic
ivermectin: - + - +
dox: - + - + - + - +
100 αNCL
size (kDa) 55 αmuSOX
70 αLMNB1
40 αGAPDH
NCL protein expression
mock
ivermectin
band intensity fold chg
p<0.1
muSOX: - + - + - + - +
fraction: nuclear cytoplasmic
F
Total RNA
no muSOX D219A
+muSOX D219A
RNA fold chg /18S
inhibitor: – mock ivermectin
gene: ACTB GAPDH 7SK
RNAPII genes
RNAPIII gene
G
RNAPII promoter occupancy
IgG
no D219A
+D219A
relative % input
inhibitor: – – mock ivermectin
promoter: ACTB GAPDH

593 **Figure S4.** Importin α/β transport links mRNA decay and transcription. (A) Western blot
594 showing the efficacy of siRNA-mediated knock down of PABPC1 and PABPC4 in
595 HCT116 cells before and after 2 hr TRAIL treatment. Caspase 3 (CASP3) cleavage
596 confirmed induction of apoptosis, while α-Tubulin (TUBA1A) served as a loading
597 control. (B) Nascent (4sU) transcription of the indicated genes in HCT116 cells
598 quantified by RT-qPCR. Fold changes calculated in reference to non-apoptotic cells
599 under otherwise identical cellular conditions. (C) RT-qPCR quantification of total RNA
600 levels in cells in (B), but with all conditions normalized to scramble siRNA-treated non-
601 apoptotic cells. (D) Changes in total RNA levels after 2 hr TRAIL treatment in HCT116
602 cells pretreated with either 25 μM ivermectin or an equal volume of ethanol for 1 hr. (E)
603 Additional analysis of data presented in Figure 4C, instead quantifying the fold change
604 in nascent transcription in non-apoptotic cells in the presence or absence of 25 μM
605 ivermectin. (F) Western blot showing nuclear and cytoplasmic expression of the
606 indicated proteins in HEK293T expressing a doxycycline (dox)-inducible form of the viral
607 endonuclease muSOX, with or without a 48 hr 1 μg/mL dox treatment. In the graph
608 below, nuclear levels of nucleolin (NCL) were quantified by band intensity in reference
609 to a lamin B1 (LMNB1) loading control, while cytoplasmic levels were calculated in
610 reference to α-Tubulin (TUBA1A). (F) RT-qPCR quantification of the change (or lack
611 thereof) in total RNA levels upon dox-inducible expression of the catalytically dead
612 D219A mutant of muSOX. (G) RNAPII occupancy at the *ACTB* and *GAPDH* promoters
613 under cellular conditions described in (F). RNA fold change values were calculated in
614 reference to *18S* rRNA. All bar graphs display mean +/- SEM with individual biological
615 replicates represented as dots. Statistically significant deviation from a null hypothesis

616 of 1 was determined using one sample t test and indicated with asterisks directly above
617 bars, while multiple t tests with the Holm-Sidak correction for multiple comparisons were
618 performed to compare mean values between groups indicated with brackets. *p<0.05,
619 **p<0.0.1, ***p<0.001.

620 **STAR METHODS**

621 **Resource Availability**

622 ***Lead Contact***

623 Further information and requests for resources and reagents should be directed to and
624 will be fulfilled by the Lead Contact, Britt Glaunsinger (glaunsinger@berkeley.edu).

625 ***Materials availability***

626 The dox-inducible muSOX-expressing cell line and rabbit polyclonal anti-muSOX
627 antibody generated in this study are both available upon request.

628 ***Data and Code Availability***

629 This study did not generate any datasets or code.

630 **Experimental model and subject details**

631 ***Cells and culture conditions***

632 Wild-type HCT116, HEK293T, and HeLa cells (all from ATCC) were obtained from the
633 UC Berkeley Tissue Culture Facility. HEK293Ts were made to stably express
634 doxycycline(dox)-inducible wild-type muSOX and its catalytically-dead D219A mutant by
635 PCR amplifying the aforementioned coding sequences from Addgene plasmids 131702
636 and 131704 using the muSOX F/R primers (see Key Resources Table) and InFusion
637 cloning these fragments into the Lenti-X™ Tet-One™ Inducible Expression System
638 digested with AgeI. Lentivirus was made for both constructs by transfecting 293T cells

639 with second generation packaging plasmids and spinfected onto 293T cells at a low
640 multiplicity of infection (MOI) as previously described (Hartenian et al., 2020). 24 hr
641 later, 350 μg/ml zeocin was added to select for transduced cells. HEK293T and HeLa
642 cells were grown in Dulbecco's Modified Eagle Medium (ThermoFisher Scientific)
643 supplemented with 10% fetal bovine serum (FBS) and 1 U/mL penicillin-streptomycin
644 (pen-strep). HCT116 cells were maintained in McCoy's (modified) 5A medium
645 (ThermoFisher Scientific) with 10% FBS and 1 U/mL pen-strep. All cells were incubated
646 at 37 ^{o}C with 5% CO_2. Cell lines were authenticated by STR analysis and determined to
647 be free of mycoplasma by PCR screening. Cells were maintained in culture in 10 cm^2
648 plates and $1x10^6$ cells were seeded into 6 well plates for all experiments except for
649 chromatin immunoprecipitations, in which $5x10^6$ cells were seeded into 10 cm^2 plates.

650 **Method Details**

651 ***siRNA nucleofections***

652 Protein knock downs were performed using the Neon Transfection System (Thermo
653 Fisher Scientific) with Dharmacon ON-TARGETplus siRNA SmartPools for the following
654 targets: Non-targeting Control Pool (scramble or scr siRNA), CASP3, CASP8, DFFB,
655 DIS3L2, EXOSC4, PNPT1, and XRN1. Custom ON-TARGETplus siRNA pools from
656 Dharmacon were also synthesized to target PABPC1 and PABPC4. For all siRNA
657 pools, cells were nucleofected according to manufacturer protocols for HCT116 cells
658 and immediately seeded into plates containing media supplemented with 10% FBS but
659 lacking pen-strep to improve cell viability post-nucleofection. A 50 nM final siRNA
660 concentration was used for pools targeting CASP3, CASP8, and DFFB (CAD), while
661 200 nM was used for knock down of XRN1 and the concurrent knock downs of

662 DIS3L2/EXOSC4/PNPT1 (66.7 nM each). For all experiments involving siRNA knock
663 downs, cells were treated and/or harvested once 80-90% confluent in each plate or well,
664 approximately 72 hr post-nucleofection, and protein knock down was confirmed by
665 western blot.

666 ***Apoptosis induction***

667 100 ng/mL TNF-related apoptosis-inducing ligand (TRAIL) was used to induce rapid
668 extrinsic apoptosis in HCT116 cells. Where indicated, HCT116 cells were pre-treated for
669 1 hr with 40 μM caspase Inhibitor Z-VAD-FMK (zVAD; Promega Corporation) or 25 μM
670 ivermectin (Millipore Sigma) before TRAIL treatment. Extrinsic apoptosis induction was
671 confirmed by observing CASP8 and CASP3 cleavage on western blots. CASP3/8
672 cleavage was quantified by disappearance in intensity of the full-sized band normalized
673 to TUBA1A or VCL using BioRad ImageLab software. Intrinsic apoptosis was induced in
674 HeLa cells with a 4 hr treatment of 10 μM raptinal (Millipore Sigma), with or without 1 hr
675 pre-treatment with 20 μM zVAD. Induction was confirmed by evidence of cytochrome c
676 release into the cytoplasm with cell fractionation and western. “Mock” treatments
677 consisted of an equal volume of solvent used to dissolve each reagent: TRAIL storage
678 and dilution buffer, DMSO, and ethanol for TRAIL, zVAD, and ivermectin, respectively.

679 ***RNA, DNA, and protein extractions***

680 Total RNA, and protein extractions were performed according to manufacturer’s
681 instructions after cells were harvested with Trizol™ reagent (ThermoFisher Scientific).
682 RNA pellets were dissolved in DEPC water and protein pellets were dissolved in 1%
683 SDS overnight at 50 °C before spinning down insoluble material at 10,000 x g for 10
684 min.

685 ***TUNEL Assay***

686 Terminal deoxynucleotidyl transferase Br-dUTP nick end labeling was performed on
687 TRAIL-treated cells using a TUNEL Assay Kit (Abcam) according to manufacturer
688 protocol. Br-dUTP incorporation was quantified by flow cytometry, analyzing the
689 elevated peak in FL2 fluorescence on a BD Accuri Flow Cytometry System using
690 FlowJo analysis software.

691 ***Quantitative reverse transcription PCR (RT-qPCR)***

692 Extracted RNA was DNAse-treated treated, primed with random nonamers, and
693 reverse-transcribed to cDNA with Avian Myeloblastosis Virus Reverse Transcriptase
694 (Promega) according to manufacturer protocols. Genes were quantified by RT-qPCR
695 using iTaq Universal SYBR Master Mix (Bio-rad Laboratories) and primers specific to
696 each gene of interest. RNA fold change values were calculated in reference to *18S* or
697 *U6* ncRNAs, as indicated on figure axes.

698 ***Western blotting***

699 Protein samples were quantified by Bradford assay according to manufacturer
700 instructions. 12.5-50 μg of protein was mixed with one third volume of 4X Laemelli
701 Sample Buffer (Bio-Rad Laboratories 1610747) and boiled at 100 ^{o}C before loading into
702 a polyacrylamide gel alongside either the PageRuler™ or PageRuler™ Plus Prestained
703 Protein Ladder (ThermoFisher Scientific). Proteins were separated by electrophoresis
704 and transferred to a nitrocellulose membrane, which was then cut into sections
705 surrounding the size of the protein of interest, allowing for multiple proteins to be
706 quantified from one gel. Membranes were then blocked with 5% non-fat dry milk in
707 TBST (1X TBS with 0.2% [v/v] Tween 20) at RT for 1 hour then incubated with relevant

708 primary antibodies diluted with 1% milk in TBST overnight at 4 ^{o}C. All primary antibodies
709 were applied at a 1:1000 dilution with the exception of the following (target, dilution):
710 RPB1, 1:500; TUBA1A, 1:500; RPB2, 1:500; RPB3, 1:10000; LMNB1, 1:1000; GAPDH,
711 1:5000; and CYTC, 1:500. After three five min TBST washes, secondary antibody
712 diluted 1:5000 with 1% milk in TBST was incubated for one hour at RT. Blots were then
713 developed, after three additional five min TBST washes, with Clarity Western ECL
714 Substrate (Bio-rad Laboratories) for five min and imaged using a ChemiDoc^{TM} MP
715 Imaging System. Each membrane section was imaged and processed separately. Band
716 intensity was quantified using Bio-Rad Image Lab software, and relative expression
717 changes were calculated after normalizing to an α-tubulin (TUBA1A), vinculin (VCL), or
718 lamin-B1 (LMNB1) loading control. For all blots that appear in figures, auto-contrast was
719 applied in Image Lab for each membrane section before the resultant image was
720 exported for publication. When appropriate, membrane sections were stripped with 15%
721 hydrogen peroxide and washed 3 times with TBST before being re-probed with a
722 primary antibody targeting a protein of similar size.

723 ***Antibody generation***

724 Polyclonal rabbit anti-muSOX antibody was made and purified by YenZym antibodies,
725 LLC from recombinant muSOX protein.

726 ***Cell Fractionations***

727 For experiments performed in apoptotic HCT116 and HeLa cells, nuclear, cytoplasmic,
728 and mitochondrial fractions were isolated using the Abcam Cell Fractionation Kit
729 according to manufacturer's instructions. Cytoplasmic and nuclear fractions of samples
730 in experiments that did not involve apoptosis were separated using the REAP method

731 (Suzuki et al., 2010). 1/5th of the total cell lysate was reserved and diluted to the same
732 volume of the cell and nuclear fractions for whole cell lysate samples. Protein was
733 extracted from 200 μL of each fraction from both methods using Trizol™ LS reagent
734 (ThermoFisher Scientific) and analyzed by western blot as described above.

735 ***4-thiouridine- (4sU)- pulse labeling***

736 4sU-pulse labeling was used to measure nascent transcription concurrently with mRNA
737 decay. 50 μM 4sU (Millipore Sigma T4509) was added to cells 20 min before
738 harvesting. Labeled transcripts contained in 25 μg of total extracted RNA were
739 biotinylated as described by Dölken (2013), using 50 μg HPDP biotin (ThermoFisher
740 Scientific). Biotinylated RNA was conjugated to Dynabeads™ MyOne™ Streptavidin C1
741 (ThermoFisher Scientific) magnetic beads for 1 hour in the dark, then the beads were
742 washed four times (twice at 65 ^{o}C and twice at RT) with wash buffer (100 mM Tris-HCl,
743 10 mM EDTA, 1 M sodium chloride, and 0.1% Tween 20) before eluting RNA off of the
744 beads twice with 5% BME in DEPC water. RNA was precipitated by adding 1/10th
745 volume of 3M sodium acetate and 2.5 volumes of ethanol and spun down at full speed
746 in a 4°C benchtop centrifuge. After a 75% ethanol wash, the 4sU-labelled RNA was
747 resuspended in 20 μL DEPC water for use in in RT-qPCR.

748 ***Chromatin immunoprecipitation (ChIP)***

749 HCT116 cells nucleofected with the relevant siRNAs were seeded onto 10 cm^2 plates.
750 72 hr post-nucleofection, cells were washed with PBS, trypsinized, washed with PBS
751 again, and fixed in 1% formaldehyde for 2.5 min before quenching with 125 mM glycine.
752 After an additional PBS wash, cells were lysed for 10 min at 4°C in lysis buffer (50 mM
753 HEPES pH 7.9, 140 mM NaCl, 1 mM EDTA, 10% [v/v] glycerol, 0.5% NP40, 0.25%

754 Triton X-100) then washed with wash buffer (10 mM Tris Cl pH 8.1, 100 mM NaCl, 1
755 mM EDTA pH 8.0) at 4 °C for 10 min. Cells were then suspended in 1 mL shearing
756 buffer (50 mM Tris Cl pH 7.5, 10 mM EDTA, 0.1% [v/v] SDS) and sonicated in a Covaris
757 S220 sonicator (Covaris Inc.) with the following parameters: peak power, 140.0; duty
758 factor, 5.0**;** cycle/burst, 200; and duration, 300 sec. Insoluble material in the shearing
759 buffer was then spun down at full speed in a 4 °C benchtop centrifuge to yield the
760 chromatin supernatant. 10 μg chromatin was rotated overnight at 4 °C with 2.5 μg or 4
761 μg ChIP-grade primary antibodies targeting RPB1 and TBP, respectively, in 500 μL
762 dilution buffer (1.1% [v/v] Triton-X-100, 1.2mM EDTA, 6.7mM Tris-HCl pH 8.0, 167mM
763 NaCl). 5 μL of each IP was reserved as an input sample before antibody was added. 20
764 μL of either Dynabeads™ Protein G or a 1:1 mixture Protein A and Protein G beads, for
765 anti-mouse and anti-rabbit antibodies, respectively, were added to each reaction and
766 rotated at 4 °C for at least 2 hr. The beads were then sequentially washed with low salt
767 immune complex wash buffer (0.1% [v/v] SDS, 1% [v/v] Triton-X-100, 2 mM EDTA, 20
768 mM Tris-HCl pH 8.0, 150 mM NaCl), high low salt immune complex wash buffer (0.1%
769 [v/v] SDS, 1% [v/v] Triton-X-100, 2 mM EDTA, 20 mM Tris-HCl pH 8, 500 mM NaCl),
770 LiCl immune complex buffer (0.25 M LiCl, 1% [v/v] NP40, 1% [v/v] deoxycholic acid,
771 1mM EDTA, 10mM Tris-HCl pH 8.0), and TE buffer (10 mM Tris-HCl pH 8.0, 1 mM
772 EDTA). All washes were 5 min in duration and performed at 4 °C. Beads and input
773 samples were then suspended in 100 μL elution buffer (150 mM NaCl, 50ug/ml
774 proteinase K) and incubated at 55 °C for 2 hr then at 65 °C for 12 hr in a thermal cycler.
775 DNA fragments were purified with an Oligo Clean and Concentrator kit (Zymo

776 Research) and % input values were quantified by RT-qPCR as previously described
777 using primers complementary to the locus of interest.

778 ***Data visualization***

779 Bar graphs were created using GraphPad Prism software and the graphical abstract
780 was made using the Bio-Render online platform.

781 **Quantification and statistical analysis**

782 Biological replicates were defined as experiments performed separately on
783 biologically distinct samples representing identical conditions and/or time points. See
784 figures and figure legends for the number (n≥3) of biological replicates performed for
785 each experiment. Criteria for the inclusion of data was based on the performance of
786 positive and negative controls within each experiment. No outliers were eliminated in
787 this study. One-sample t-tests were performed on control and experimental groups for
788 which mean fold change values were calculated, comparing these values to the null
789 hypothesis of 1. T tests corrected for multiple comparison with the Holm-Sidak were
790 also performed comparing means between control and experimental groups, signified
791 by brackets spanning the two groups being compared. All statistical analyses were
792 performed using GraphPad Prism 8.

793 **Key Resources Table**

REAGENT or RESOURCE	SOURCE	IDENTIFIER
Antibodies		
Anti-RNA polymerase II CTD repeat YSPTSPS antibody (clone 8WG16)	Abcam	Cat#ab817
Anti-RNA polymerase II CTD repeat YSPTSPS (phospho S2) antibody	Abcam	Cat#ab5095
Anti-RNA polymerase II CTD repeat YSPTSPS (phospho S5) antibody	Abcam	Cat#ab5131
Anti-alpha Tubulin antibody	Abcam	Cat#ab7291
POLR2B (RPB2) Antibody (clone E-12)	Santa Cruz Biotechnology	Cat#sc-166803

Anti-RPB3 antibody (clone EPR13294B)	Abcam	Cat#ab182150
POLR2D (RPB4) Polyclonal Antibody	ThermoFisher Scientific	Cat#PA5-35954
Anti-Vinculin antibody	Abcam	Cat#ab91459
Anti-PNPT1 antibody	Abcam	Cat#ab96176
Anti-RRP41 (EXOSC4) antibody	Abcam	Cat#ab137250
DIS3L2 Antibody	Novus Biologicals	Cat#NBP184740
Anti-Lamin B1 antibody	Abcam	Cat# ab133741
Anti-GAPDH antibody (clone 6C5)	Abcam	Cat# ab8245
Caspase-8 (clone D35G2) Rabbit mAb	Cell Signaling Technology	Cat#4790
Caspase-3 Antibody	Cell Signaling Technology	Cat#9662
XRN1 Antibody	Bethyl Laboratories	Cat#A400-433A
Anti-DFFB antibody	Abcam	Cat#ab69438
PABP1 Antibody	Cell Signaling Technology	Cat#4992
PABP4 Antibody	Bethyl Laboratories	Cat#A301-466A
C23 (NCL) Antibody (clone MS-3)	Santa Cruz Biotechnology	Cat#sc-8031
PARP Antibody	Cell Signaling Technology	Cat#9542
BID Antibody (clone 5C9)	Santa Cruz Biotechnology	Cat#sc-56025
Anti-TATA binding protein TBP antibody (clone mAbcam 51841)	Abcam	Cat#ab51841
Cytochrome c (clone D18C7) Rabbit mAb	Cell Signaling Technology	Cat#11940
Anti-VDAC1 / Porin antibody	Abcam	Cat# ab15895
Polyclonal rabbit ant-muSOX antibody	This paper	N/A
Chemicals, Peptides, and Recombinant Proteins		
Trizol™ Reagent	ThermoFisher Scientific	Cat#15596026
Trizol™ LS Reagent	ThermoFisher Scientific	Cat#10296028
TURBO™ DNase	ThermoFisher Scientific	Cat#AM2238
Avian Myeloblastosis Virus Reverse Transcriptase	Promega Corporation	Cat#M5108
iTaq Universal SYBR Master Mix	Bio-Rad Laboratories	Cat#1725122
Dynabeads™ Protein G	ThermoFisher Scientific	Cat#10003D

Dynabeads™ Protein A	ThermoFisher Scientific	Cat#10002D
Dynabeads® MyOne™ Streptavidin C1	ThermoFisher Scientific	Cat#
EZ-link™ HPDP-biotin	ThermoFisher Scientific	Cat#21341
Caspase Inhibitor Z-VAD-FMK	Promega Corporation	Cat#G7231
Ivermectin	Millipore Sigma	Cat#I8898
Raptinal	Millipore Sigma	Cat#SML1745
Dulbecco's Modified Eagle Medium	ThermoFisher Scientific	Cat#12800082
McCoy's (modified) 5A medium	ThermoFisher Scientific	Cat#16600082
Fetal Bovine Serum	VWR	Cat#89510-186
PageRuler™ Prestained Protein Ladder	ThermoFisher Scientific	Cat#26616
PageRuler™ Plus Prestained Protein Ladder	ThermoFisher Scientific	Cat#26620
Clarity Western ECL Substrate	Bio-Rad Laboratories	Cat#1705061
Critical Commercial Assays		
TUNEL Assay Kit - BrdU-Red	Abcam	Cat#ab66110
Cell Fractionation Kit	Abcam	Cat#ab109719
Bio-Rad Protein Assay Kit II	Bio-Rad Laboratories	Cat#5000002
Oligo Clean & Concentrator Kit	Zymo Research	Cat#D4060
In-Fusion® HD Cloning Kit	Takara Bio USA	Cat#639650
Lenti-X™ Tet-On® 3G Inducible Expression System	Takara Bio USA	Cat#631187
Neon Transfection System	ThermoFisher Scientific	Cat#MPK5000
Experimental Models: Cell Lines		
Human: HCT116 cells	ATCC	CCL-247
Human: 293T/17 cells	ATCC	CRL-11268
Human: HeLa Cells	ATCC	CCL-2
Oligonucleotides		
PABPC1 siRNA #1	Gilbertson et al. 2018	GAAAGGAGCT CAATGGAAA
PABPC1 siRNA #2	Gilbertson et al. 2018	GGACAAATCCA TTGATAAT
PABPC4 siRNA #1	Gilbertson et al. 2018	AGGAGAGAAU UAGUCGAUAU CAGGG

PABPC4 siRNA #2	Gilbertson et al. 2018	GGAAUUCAAC UCAAGGUUUG AAGAC
muSOX F	This paper	TCCCGTATACA CCGGTATGTG GAGCCACCCC
muSOX R	This paper	ATCCGCCGGC ACCGGTTTAGG GGGTTATGGG
ON-TARGETplus Non-targeting Control Pool	Horizon Discovery Group	Cat#D-001810-10
SMARTpool: ON-TARGETplus DIS3L2 siRNA	Horizon Discovery Group	Cat#L-018715-01
SMARTpool: ON-TARGETplus Human EXOSC4 siRNA	Horizon Discovery Group	Cat#L-013760-00
SMARTpool: ON-TARGETplus Human PNPT1 siRNA	Horizon Discovery Group	Cat#L-019454-01
SMARTpool: ON-TARGETplus XRN1 siRNA	Horizon Discovery Group	Cat#L-013754-01
SMARTpool: ON-TARGETplus CASP3 siRNA	Horizon Discovery Group	Cat#L-004307-00
SMARTpool: ON-TARGETplus CASP8 siRNA	Horizon Discovery Group	Cat#L-003466-00
ON-TARGETplus DFFB siRNA SMARTpool	Horizon Discovery Group	Cat#L-004425-00
See Table S1 for qPCR primers		
Software and Algorithms		
Prism 8	GraphPad	https://www.graphpad.com/scientific-software/prism/
FlowJo	BD	https://www.flowjo.com/solutions/flowjo
Image Lab Software	Bio-Rad Laboratories	Cat#1709690

794

795 **REFERENCES**

796 Abernathy, E., Clyde, K., Yeasmin, R., Krug, L.T., Burlingame, A., Coscoy, L.,

797 Glaunsinger, B., 2014. Gammaherpesviral Gene Expression and Virion

798 Composition Are Broadly Controlled by Accelerated mRNA Degradation. PLoS

799 Pathog. 10, e1003882.
800 Abernathy, E., Gilbertson, S., Alla, R., Glaunsinger, B., 2015. Viral nucleases induce an
801 mRNA degradation-transcription feedback loop in mammalian cells. Cell Host
802 Microbe 18, 243–253.
803 Albeck, J.G., Burke, J.M., Aldridge, B.B., Zhang, M., Lauffenburger, D.A., Sorger, P.K.,
804 2008. Quantitative Analysis of Pathways Controlling Extrinsic Apoptosis in Single
805 Cells. Mol. Cell 30, 11–25.
806 Bentley, D.L., 2014. Coupling mRNA processing with transcription in time and space.
807 Nat. Rev. Genet. 15, 163–175.
808 Bernstein, P., Peltz, S.W., Ross, J., 1989. The poly(A)-poly(A)-binding protein complex
809 is a major determinant of mRNA stability in vitro. Mol. Cell. Biol. 9, 659–670.
810 Braun, K.A., Young, E.T., 2014. Coupling mRNA Synthesis and Decay. Mol. Cell. Biol.
811 34, 4078–4087.
812 Bregman, A., Avraham-kelbert, M., Barkai, O., Duek, L., Guterman, A., Choder, M.,
813 2011. Promoter Elements Regulate Cytoplasmic mRNA Decay. Cell 147, 1473–
814 1483.
815 Brook, M., Gray, N.K., 2012. The role of mammalian poly(A)-binding proteins in co-
816 ordinating mRNA turnover. Biochem. Soc. Trans. 40, 856–864.
817 Buratowski, S., Hahn, S., Guarente, L., Sharp, P.A., 1989. Five intermediate complexes
818 in transcription initiation by RNA polymerase II. Cell 56, 549–561.
819 Caruso, S., Poon, I.K.H., 2018. Apoptotic cell-derived extracellular vesicles: More than
820 just debris. Front. Immunol. 9, 1486.
821 Collart, M.A., Stmhp, K., 1994. NOTl (CDC39), NOT2 (CDC36), NOT3 , and N0T4

822 encode a global-negative regulator of transcription that differentially affects TATA-
823 element utilization 2, 525–537.
824 Dantonel, J.C., Murthy, K.G.K., Manjey, J.L., Tora, L., 1997. Transcription factor TFIID
825 recruits factor CPSF for formation of 3 end of mRNA. Nature 389, 399–402.
826 Denis, C.L., 1984. Identification of new genes involved in the regulation of yeast alcohol
827 dehydrogenase II. Genetics 108, 833–844.
828 Dölken, L., 2013. High Resolution Gene Expression Profiling of RNA Synthesis,
829 Processing, and Decay by Metabolic Labeling of Newly Transcribed RNA Using 4-
830 Thiouridine. In: Bailer, S.M., Lieber, D. (Eds.), Virus-Host Interactions: Methods and
831 Protocols. Humana Press, Totowa, NJ, pp. 91–100.
832 Düring, L., Thorsen, M., Petersen, D.S.N., Køster, B., Jensen, T.H., Holmberg, S., 2012.
833 MRN1 Implicates Chromatin Remodeling Complexes and Architectural Factors in
834 mRNA Maturation. PLoS One 7, 1–13.
835 El-Brolosy, M.A., Kontarakis, Z., Rossi, A., Kuenne, C., Günther, S., Fukuda, N., Kikhi,
836 K., Boezio, G.L.M., Takacs, C.M., Lai, S.L., Fukuda, R., Gerri, C., Giraldez, A.J.,
837 Stainier, D.Y.R., 2019. Genetic compensation triggered by mutant mRNA
838 degradation. Nature 568, 193–197.
839 Enari, M., Sakahira, H., Yokoyama, H., Okawa, K., Iwamatsu, A., Nagata, S., 1998.
840 Cleavage of CAD inhibitor in CAD activation and DNA degradation during
841 apoptosis. Nature 391, 43–50.
842 Gilbertson, S., Federspiel, J.D., Hartenian, E., Cristea, I.M., Glaunsinger, B., 2018.
843 Changes in mRNA abundance drive shuttling of RNA binding proteins, linking
844 cytoplasmic RNA degradation to transcription. Elife 7, 1–26.

845 Gö, D., 1998. MEDAL REVIEW Transport into and out of the cell nucleus. EMBO J. 17,
846 2721–2727.
847 Goss, D.J., Kleiman, F.E., 2013. Poly(A) binding proteins: Are they all created equal?
848 Wiley Interdiscip. Rev. RNA 4, 167–179.
849 Haimovich, G., Medina, D.A., Causse, S.Z., Garber, M., Millán-Zambrano, G., Barkai,
850 O., Chávez, S., Pérez-Ortín, J.E., Darzacq, X., Choder, M., 2013. Gene expression
851 is circular: Factors for mRNA degradation also foster mRNA synthesis. Cell 153.
852 Hartenian, E., Gilbertson, S., Federspiel, J.D., Cristea, I.M., Glaunsinger, B.A., 2020.
853 RNA decay during gammaherpesvirus infection reduces RNA polymerase II
854 occupancy of host promoters but spares viral promoters. PLoS Pathog. 16,
855 e1008269–e1008269.
856 Hartenian, E., Glaunsinger, B.A., 2019. Feedback to the central dogma: cytoplasmic
857 mRNA decay and transcription are interdependent processes. Crit. Rev. Biochem.
858 Mol. Biol. 54, 385–398.
859 Harwig, A., Landick, R., Berkhout, B., 2017. The battle of RNA synthesis: Virus versus
860 host. Viruses 9, 1–18.
861 Helenius, K., Yang, Y., Tselykh, T. V., Pessa, H.K.J., Frilander, M.J., Mäkelä, T.P.,
862 2011. Requirement of TFIIH kinase subunit Mat1 for RNA Pol II C-terminal domain
863 Ser5 phosphorylation, transcription and mRNA turnover. Nucleic Acids Res. 39,
864 5025–5035.
865 Houseley, J., Tollervey, D., 2009. The Many Pathways of RNA Degradation. Cell 136,
866 763–776.
867 Ivanov, A., Mikhailova, T., Eliseev, B., Yeramala, L., Sokolova, E., Susorov, D.,

868 Shuvalov, A., Schaffitzel, C., Alkalaeva, E., 2016. PABP enhances release factor
869 recruitment and stop codon recognition during translation termination. Nucleic
870 Acids Res. 44, 7766–7776.
871 Jones, C.I., Zabolotskaya, M.V., Newbury, S.F., 2012. The 5′ → 3′ exoribonuclease
872 XRN1/Pacman and its functions in cellular processes and development. Wiley
873 Interdiscip. Rev. RNA 3, 455–468.
874 Kimura, M., Kose, S., Okumura, N., Imai, K., Furuta, M., Sakiyama, N., Tomii, K.,
875 Horton, P., Takao, T., Imamoto, N., 2013. Identification of cargo proteins specific
876 for the nucleocytoplasmic transport carrier transportin by combination of an in vitro
877 transport system and stable isotope labeling by amino acids in cell culture (SILAC)-
878 based quantitative proteomics. Mol. Cell. Proteomics 12, 145–157.
879 Kumar, G.R., Glaunsinger, B.A., 2010. Nuclear Import of Cytoplasmic Poly(A) Binding
880 Protein Restricts Gene Expression via Hyperadenylation and Nuclear Retention of
881 mRNA. Mol. Cell. Biol. 30, 4996–5008.
882 Kumar, G.R., Shum, L., Glaunsinger, B.A., 2011. Importin -Mediated Nuclear Import of
883 Cytoplasmic Poly(A) Binding Protein Occurs as a Direct Consequence of
884 Cytoplasmic mRNA Depletion. Mol. Cell. Biol. 31, 3113–3125.
885 Łabno, A., Tomecki, R., Dziembowski, A., 2016. Cytoplasmic RNA decay pathways -
886 Enzymes and mechanisms. Biochim. Biophys. Acta - Mol. Cell Res. 1863, 3125–
887 3147.
888 Lee, Y.J., Glaunsinger, B.A., 2009. Aberrant herpesvirus-induced polyadenylation
889 correlates with cellular messenger RNA destruction. PLoS Biol. 7, e1000107.
890 Liu, X., Fu, R., Pan, Y., Meza-sosa, K.F., Zhang, Z., Liu, X., Fu, R., Pan, Y., Meza-sosa,

891 K.F., Zhang, Z., Lieberman, J., 2018. PNPT1 Release from Mitochondria during
892 Apoptosis Triggers Decay of Poly(A) RNAs. Cell 1–15.
893 Lotan, R., Bar-On, V.G., Harel-Sharvit, L., Duek, L., Melamed, D., Choder, M., 2005.
894 The RNA polymerase II subunit Rpb4p mediates decay of a specific class of
895 mRNAs. Genes Dev. 19, 3004–3016.
896 Lotan, R., Goler-Baron, V., Duek, L., Haimovich, G., Choder, M., 2007. The Rpb7p
897 subunit of yeast RNA polymerase II plays roles in the two major cytoplasmic mRNA
898 decay mechanisms. J. Cell Biol. 178, 1133–1143.
899 Louder, R.K., He, Y., López-Blanco, J.R., Fang, J., Chacón, P., Nogales, E., 2016.
900 Structure of promoter-bound TFIID and model of human pre-initiation complex
901 assembly. Nature 531, 604–609.
902 Lu, Y., Luo, Z., Bregman, D.B., 2002. Rna polymerase II large subunit is cleaved by
903 caspases during DNA damage-induced apoptosis. Biochem. Biophys. Res.
904 Commun. 296, 954–961.
905 Ma, Z., Zhu, P., Shi, H., Guo, L., Zhang, Q., Chen, Y., Chen, S., Zhang, Z., Peng, J.,
906 Chen, J., 2019. PTC-bearing mRNA elicits a genetic compensation response via
907 Upf3a and COMPASS components. Nature 568, 259–263.
908 Nagata, S., Hanayama, R., Kawane, K., 2010. Autoimmunity and the Clearance of Dead
909 Cells. Cell 140, 619–630.
910 Narayanan, K., Makino, S., 2013. Interplay between viruses and host mRNA
911 degradation. Biochim. Biophys. Acta - Gene Regul. Mech. 1829, 732–741.
912 Noonberg, S.B., Scott, G.K., Benz, C.C., 1996. Evidence of post-transcriptional
913 regulation of U6 small nuclear RNA. J. Biol. Chem. 271, 10477–10481.

914 Palchaudhuri, R., Lambrecht, M.J., Botham, R.C., Partlow, K.C., van Ham, T.J., Putt,
915 K.S., Nguyen, L.T., Kim, S.H., Peterson, R.T., Fan, T.M., Hergenrother, P.J., 2015.
916 A Small Molecule that Induces Intrinsic Pathway Apoptosis with Unparalleled
917 Speed. Cell Rep. 13, 2027–2036.
918 Rivas, H.G., Schmaling, S.K., Gaglia, M.M., 2016. Shutoff of host gene expression in
919 influenza A virus and herpesviruses: Similar mechanisms and common themes.
920 Viruses 8, 1–26.
921 Shandilya, J., Roberts, S.G.E., 2012. The transcription cycle in eukaryotes: From
922 productive initiation to RNA polymerase II recycling. Biochim. Biophys. Acta - Gene
923 Regul. Mech. 1819, 391–400.
924 Singh, P., James, R.S., Mee, C.J., Morozov, I.Y., Singh, P., James, R.S., Mee, C.J.,
925 Morozov, I.Y., Singh, P., James, R.S., Mee, C.J., Morozov, I.Y., 2019. mRNA levels
926 are buffered upon knockdown of RNA decay and translation factors via adjustment
927 of transcription rates in human HepG2 cells adjustment of transcription rates in
928 human HepG2 cells. RNA Biol. 16, 1147–1155.
929 Stewart, M., 2007. Molecular mechanism of the nuclear protein import cycle. Nat. Rev.
930 Mol. Cell Biol. 8, 195–208.
931 Suffert, G., Malterer, G., Hausser, J., Viiliäinen, J., Fender, A., Contrant, M., Ivacevic,
932 T., Benes, V., Gros, F., Voinnet, O., Zavolan, M., Ojala, P.M., Haas, J.G., Pfeffer,
933 S., 2011. Kaposi's sarcoma herpesvirus microRNAs target caspase 3 and regulate
934 apoptosis. PLoS Pathog. 7, e1002405.
935 Sun, M., Schulz, D., Pirkl, N., Etzold, S., Larivie, L., Maier, K.C., Seizl, M., Tresch, A.,
936 Cramer, P., 2012. Comparative dynamic transcriptome analysis (cDTA) reveals

937 mutual feedback between mRNA synthesis and degradation. Genome Res. 22,
938 1350–1359.
939 Suzuki, K., Bose, P., Leong-Quong, R.Y., Fujita, D.J., Riabowol, K., 2010. REAP: A two
940 minute cell fractionation method. BMC Res. Notes 3, 294.
941 Tabtieng, T., Degterev, A., Gaglia, M.M., 2018. Caspase-Dependent Suppression of
942 Type I Interferon Signaling. Virology 92, 1–17.
943 Tarun, J., Wells, S.E., Deardorff, J.A., Sachs, A.B., 1997. Translation initiation factor
944 eIF4G mediates in vitro poly(A) tail- dependent translation. Proc. Natl. Acad. Sci. U.
945 S. A. 94, 9046–9051.
946 Thomas, M.P., Liu, X., Whangbo, J., McCrossan, G., Sanborn, K.B., Basar, E., Walch,
947 M., Lieberman, J., 2015. Apoptosis Triggers Specific, Rapid, and Global mRNA
948 Decay with 3' Uridylated Intermediates Degraded by DIS3L2. Cell Rep. 11, 1079–
949 1089.
950 Tucker, M., Valencia-Sanchez, M.A., Staples, R.R., Chen, J., Denis, C.L., Parker, R.,
951 2001. The transcription factor associated Ccr4 and Caf1 proteins are components
952 of the major cytoplasmic mRNA deadenylase in Saccharomyces cerevisiae. Cell
953 104, 377–386.
954 Wagstaff, K.M., Sivakumaran, H., Heaton, S.M., Harrich, D., Jans, D.A., 2012.
955 Ivermectin is a specific inhibitor of importin α/β-mediated nuclear import able to
956 inhibit replication of HIV-1 and dengue virus. Biochem. J. 443, 851–856.
957 Walker, A.P., Fodor, E., 2019. Interplay between Influenza Virus and the Host RNA
958 Polymerase II Transcriptional Machinery. Trends Microbiol. 27, 398–407.
959 Walsh, D., Mathews, M.B., Mohr, I., 2013. Tinkering with Translation : Protein Synthesis.

960 Cold Spring Harb. Perspect. Biol. 5, 1–30.
961 Walsh, J.G., Cullen, S.P., Sheridan, C., Lüthi, A.U., Gerner, C., Martin, S.J., 2008.
962 Executioner caspase-3 and caspase-7 are functionally distinct proteases. Proc.
963 Natl. Acad. Sci. U. S. A. 105, 12815–12819.
964 Wang, Z., Day, N., Trifillis, P., Kiledjian, M., 1999. An mRNA Stability Complex
965 Functions with Poly(A)-Binding Protein To Stabilize mRNA In Vitro. Mol. Cell. Biol.
966 19, 4552–4560.
967 Wilkinson, M.F., 2019. Genetic paradox explained by nonsense (NITC: nonsense-
968 induced transcriptional compentsation). Nature 568, 179–180.
969 Zhang, A., Hildreth, R.L., Colberg-Poley, A.M., 2013. Human Cytomegalovirus Inhibits
970 Apoptosis by Proteasome-Mediated Degradation of Bax at Endoplasmic Reticulum-
971 Mitochondrion Contacts. J. Virol. 87, 5657–5668.
972 Zhou, X., Jiang, W., Liu, Z., Liu, S., Liang, X., 2017. Virus infection and death receptor-
973 mediated apoptosis. Viruses 9, 316.
974

Table S1. qPCR primers

Gene/	**Forward sequence**	**Reverse sequence**
RT-qPCR		
ACTB	CATGTACGTTGCTATCCAGGC	CTCCTTAATGTCACGCACGAT
GAPDH	CAACGGATTTGGTCGTATTGG	GCAACAATATCCACTTTACCAGAGTTAA
EEF1A	TGTCGTCATTGGACACGTAGA	ACGCTCAGCTTTCAGTTTATCC
PP1A	TCCTGGCATCTTGTCCATG	CCATCCAACCACTCAGTCTTG
CHMP2A	CGCGAGCGACAGAAACTAGAG	CCCGCATCAATACAAACTTGC
DDX6	CAGGAACATCGAAATCGTG	TCCAATACGATGGAGATAGG
RPB2	CCTGAGGGTGACGAGGATCT	GTGCTTCCATTCCGCATACAG
RPLP0	GCAGCATCTACAACCCTGAAG	CACTGGCAACATTGCGGAC
U6	CGCTTCGGCAGCACATATAC	AAAATATGGAACGCTTCACGA
7SK	CCCCTGCTAGAACCTCCAAAC	CACATGCAGCGCCTCATTT
7SL	ATCGGGTGTCCGCACTAAGTT	CAGCACGGGAGTTTTGACCT
5S	GGCCATACCACCCTGAACGC	CAGCACCCGGTATTCCCAGG
18S	GTAACCCGTTGAACCCCATT	CCATCCAATCGGTAGTAGCG
ChIP		
ACTB promoter	CCGAAAGTTGCCTTTTATGG	GCCGCTGGGTTTTATAGGG
GAPDH promoter	TACTAGCGGTTTTACGGGCG	TCGAACAGGAGGAGCAGAGACCGA